

COMPUTING THE RIEMANNIAN LOGARITHM ON THE STIEFEL MANIFOLD: METRICS, METHODS AND PERFORMANCE

RALF ZIMMERMANN* AND KNUT HÜPER†

Abstract. We address the problem of computing Riemannian normal coordinates on the real, compact Stiefel manifold of orthonormal frames. The Riemannian normal coordinates are based on the so-called Riemannian exponential and the associated Riemannian logarithm map and enable to transfer almost any computational procedure to the realm of the Stiefel manifold. To compute the Riemannian logarithm is to solve the (local) geodesic endpoint problem. Instead of restricting the consideration to geodesics with respect to a single selected metric, we consider a family of Riemannian metrics introduced by Hüper, Markina and Silva-Leite that includes the Euclidean and the canonical metric as prominent examples.

As main contributions, we provide (1) a unified, structured, reduced formula for the Stiefel geodesics. The formula is unified in the sense that it works for the full family of metrics under consideration. It is structured in the sense that it relies on matrix exponentials of skew-symmetric matrices exclusively. It is reduced in relation to the dimension of the matrices of which matrix exponentials have to be calculated. We provide (2) a unified method to tackle the geodesic endpoint problem numerically and (3) we improve the existing Riemannian log algorithm under the canonical metric in terms of the computational efficiency. The findings are illustrated by means of numerical examples, where the novel algorithms prove to be the most efficient methods known to this date.

Key words. Stiefel manifold, Riemannian logarithm, geodesic endpoint problem, Riemannian computing

AMS subject classifications. 15A16, 15B10, 33B30, 33F05, 53-04, 65F60

1. Introduction. Riemannian computing methods have established themselves as important tools in a large variety of applications, including computer vision, machine learning, and optimization, see [1, 2, 3, 11, 12, 21, 28, 29] and the anthologies [22, 33]. They also gain increasing attention in statistics and data science [27] and in numerical methods for differential equations [4, 8, 14, 19, 43].

One way to enable the practical execution of data processing methods on a curved manifold \mathcal{M} is via working in local coordinates. This holds among others for basic tasks like averaging, clustering, interpolation and optimization. Of special importance are the *Riemannian normal coordinates*, as they are *radially isometric* [20, §5]. The Riemannian normal coordinates rely on the *Riemannian exponential* and the *Riemannian logarithm*, which are local diffeomorphisms: The exponential at a manifold location $p \in \mathcal{M}$ sends a tangent vector v (i.e., the velocity vector of a manifold curve) to the endpoint $q = c(1)$ of a geodesic curve c that starts from $p = c(0)$ with velocity $v = \dot{c}(0)$. The Riemannian logarithm at p maps a manifold location $q \in \mathcal{M}$ to the starting velocity vector v of a geodesic c that connects $p = c(0)$ and $q = c(1)$. [Figure 1](#) illustrates this process. Hence, the Riemannian logarithm is associated with the *geodesic endpoint problem*:

“Given $p, q \in \mathcal{M}$, find a geodesic arc that connects p and q .”

In this work, we tackle the local geodesic endpoint problem on the Stiefel manifold of orthonormal frames. Geodesics depend on the way the length of velocity vectors of curves are measured and thus on the Riemannian metric. Popular choices for metrics on the Stiefel manifold are the *Euclidean metric* and the *canonical metric*. These will

*Department of Mathematics and Computer Science, University of Southern Denmark (SDU), Odense, Denmark, (zimmermann@imada.sdu.dk)

†Institute of Mathematics, Julius-Maximilians-Universität, Würzburg, Germany, (hueper@mathematik.uni-wuerzburg.de)

be detailed in [Section 2](#). Rather than restricting the considerations to either of these two, we work with the one-parameter family of metrics that is introduced in [\[17\]](#). This family contains the Euclidean and the canonical Stiefel metric as special cases.

Original contributions.

- We start from the results of [\[11\]](#) and [\[18\]](#) and derive a unified formula for the Stiefel geodesics and thus for the Stiefel exponential. Here, unified is to be understood in the sense that the formula works for all metrics in the one-parameter family under consideration. Moreover it features the same skew-symmetric structure as exhibited by the canonical geodesics and comes at roughly the same computational costs.
- We provide new theoretical insights on the structure of the matrices that come into consideration as candidate solutions for the Stiefel geodesic endpoint problem. For rectangular matrices of dimensions $(n \times p)$, $n \gg p$, this reduces the endpoint problem to finding suitable $(p \times p)$ -orthogonal matrices.
- We provide efficient algorithms for computing the Riemannian logarithm in a unified way for the full one-parameter family of metrics of [\[17\]](#).
- For the special case of the canonical metric, the endpoint problem features a simplified structure that was exploited in [\[40\]](#). We refine this approach and thus accelerate the existing method.
- We juxtapose the various methods by means of numerical experiments, where the new methods prove to outperform both their predecessors from [\[7, 40\]](#) as well as Newton-based approaches.

Related work. The reference [\[29, section 5\]](#) tackles the local geodesic endpoint problem for the canonical metric via a Riemannian optimization approach; [\[40\]](#) also works in the setting of the canonical metric and provides a matrix-algebraic algorithm based on the Baker-Campbell-Hausdorff formula with guaranteed local linear convergence. An algorithm for computing the Stiefel logarithm for the Euclidean metric is considered in [\[7\]](#) and is based on the general “shooting method”, see [\[32, section 6.5\]](#). The thesis [\[35\]](#) considers single-shooting and multiple-shooting methods based on Newton’s method to solve the geodesic endpoint problem under the canonical metric. It also features an algorithm for computing global Stiefel geodesics that is based on the “leapfrog method” of [\[26\]](#) for general manifolds, see also the associated preprint [\[36\]](#). This approach requires methods that tackle the geodesic endpoint problem locally, i.e., for input points that are close enough to each other, as building blocks. The notion of being “close enough” depends on geometric quantities (like the injectivity radius) but also on the numerical algorithm that is applied to the problem.

Notational specifics. For $p \in \mathbb{N}$, the $(p \times p)$ -identity matrix is denoted by $I_p \in \mathbb{R}^{p \times p}$, or simply I , if the dimension is clear. The $(p \times p)$ -orthogonal group, i.e., the set of all square orthogonal matrices is denoted by

$$O(p) = \{\phi \in \mathbb{R}^{p \times p} \mid \phi^T \phi = \phi \phi^T = I_p\}.$$

The standard matrix exponential and matrix logarithm are denoted by

$$\exp_m(X) := \sum_{j=0}^{\infty} \frac{X^j}{j!}, \quad \log_m(I + X) := \sum_{j=1}^{\infty} (-1)^{j+1} \frac{X^j}{j}.$$

The sets of symmetric and skew-symmetric $(p \times p)$ -matrices are $\text{sym}(p) = \{A \in \mathbb{R}^{p \times p} \mid A^T = A\}$ and $\text{skew}(p) = \{A \in \mathbb{R}^{p \times p} \mid A^T = -A\}$, respectively. Overloading this notation, $\text{sym}(A) = \frac{1}{2}(A + A^T)$, $\text{skew}(A) = \frac{1}{2}(A - A^T)$ denote the symmetric and skew-symmetric parts of a matrix A .

Unless stated otherwise, when we employ the QR-decomposition of a rectangular matrix $A \in \mathbb{R}^{n \times p}$, we implicitly assume that $n \geq p$ and work with the ‘compact’ QR-decomposition $A = QR$, with $Q \in \mathbb{R}^{n \times p}$, $R \in \mathbb{R}^{p \times p}$.

2. The Stiefel manifold. This section reviews the essential aspects of Stiefel manifolds in regards of numerical, matrix-algorithmic applications. For additional background, see [2, 11, 43]. For featured applications, see, e.g., [5, 9, 16, 38].

The *Stiefel manifold* $St(n, p)$ is the set of rectangular, column-orthonormal n -by- p matrices,

$$St(n, p) := \{U \in \mathbb{R}^{n \times p} \mid U^T U = I_p\}, \quad p \leq n.$$

Observe that this matrix set is the pre-image $St(n, p) = F^{-1}(0)$ of the function $F : \mathbb{R}^{n \times p} \rightarrow \text{sym}(p)$, $Y \mapsto Y^T Y - I_p$. By the regular value theorem, it is a differentiable manifold of dimension $np - \frac{1}{2}p(p+1)$.

The *tangent space* $T_U St(n, p)$ at $U \in St(n, p)$ is represented as

$$T_U St(n, p) = \{\Delta \in \mathbb{R}^{n \times p} \mid U^T \Delta \in \text{skew}(p)\}.$$

For brevity, we will often write T_U instead of $T_U St(n, p)$. Every tangent vector $\Delta \in T_U$ may be written as

$$\begin{aligned} (1) \quad \Delta &= UA + (I - UU^T)T, & A \in \text{skew}(p), \quad T \in \mathbb{R}^{n \times p} \text{ arbitrary,} \\ (2) \quad \Delta &= UA + U^\perp H, & A \in \text{skew}(p), \quad H \in \mathbb{R}^{(n-p) \times p} \text{ arbitrary.} \end{aligned}$$

In the latter case, $U^\perp \in St(n, n-p)$ is an orthonormal completion such that the matrix $(U \mid U^\perp)$ is orthogonal. Any matrix $W \in \mathbb{R}^{n \times p}$ can be projected onto T_U by

$$(3) \quad \Pi_U(W) = W - U \text{sym}(U^T W),$$

see [11, eqs. (2.3), (2.4)].

In order to turn $St(n, p)$ into a *Riemannian manifold* [20], a metric, i.e., an inner product $\langle \cdot, \cdot \rangle_U$ with associated norm $\|\cdot\|_U = \sqrt{\langle \cdot, \cdot \rangle_U}$ on the tangent spaces T_U must be defined for all $U \in St(n, p)$. Given a metric, the length of a curve $C : [a, b] \rightarrow St(n, p)$ is $L(C) := \int_a^b \|\dot{C}(t)\|_{C(t)} dt$. Candidates for length-minimizing curves are called *geodesics* and are locally uniquely determined by an ordinary initial value problem when specifying a starting point $C(0)$ and a starting velocity $\dot{C}(t)$, [20, §6]. It is obvious that geodesics depend on the underlying Riemannian metric.

Geodesics give rise to the Riemannian exponential map. On the Stiefel manifold, the Riemannian exponential at a base point $U \in St(n, p)$ sends a Stiefel tangent vector Δ to the endpoint $C(1) = \tilde{U} \in St(n, p)$ of a geodesic $t \mapsto C_{U, \Delta}(t)$ that starts from $C(0) = U$ with velocity vector $\dot{C}(0) = \Delta$,

$$\text{Exp}_U(\Delta) := C_{U, \Delta}(1).$$

As a consequence, $\text{Exp}_U(t\Delta) = C_{U, \Delta}(t)$ for $t \in [0, 1]$. Knowing the Riemannian exponential is knowing the geodesics and vice versa.

The Riemannian exponential is locally invertible. The inverse is called the *Riemannian logarithm* and is denoted

$$(4) \quad \text{Log}_U : St(n, p) \ni \tilde{U} \mapsto \text{Log}_U(\tilde{U}) := \text{Exp}_U^{-1}(\tilde{U}) \in T_U St(n, p).$$

More precisely, $\text{Log}_U(\tilde{U})$ is well defined for all \tilde{U} within the *injectivity radius* $r_{St}(U)$ of $St(n, p)$ at U . The injectivity radius at U is the Riemannian distance of U to

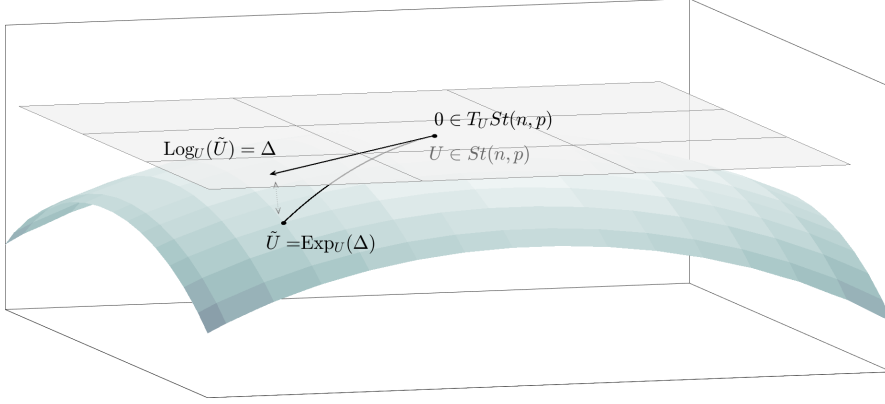


FIG. 1. (cf. Section 2) Conceptual visualization of the Stiefel manifold $St(n, p)$ (curved surface) and associated tangent space $T_U St(n, p)$ (shaded plane). The Riemannian exponential sends a tangent vector Δ from $T_U St(n, p)$ to the endpoint \tilde{U} of the geodesic $C_{U, \Delta} : [0, 1] \rightarrow St(n, p)$ with initial values $C_{U, \Delta}(0) = U, \dot{C}_{U, \Delta}(0) = \Delta$. The Riemannian logarithm inverts this process.

its cut locus C_U . The cut locus, in turn, is the set of points beyond which the geodesics starting from U cease to be length-minimizing [10, p. 271]. Combined, the Riemannian logarithm and exponential provide the *Riemannian normal coordinates*, which allow to map data points back and forth between the curved manifold and the flat tangent space, see Figure 1. This is crucial for all data processing operations on manifolds (optimization, interpolation, averaging, clustering,...). The Riemannian normal coordinates are special in that they are length-preserving along geodesic rays; one speaks of radial isometries.

The Euclidean and the canonical metric and generalizations. Let $U \in St(n, p)$ and let $\Delta = UA + U^\perp H, \tilde{\Delta} = U\tilde{A} + U^\perp \tilde{H} \in T_U$. Here and in the following, $A = U^T \Delta, \tilde{A} = U^T \tilde{\Delta} \in \text{skew}(p)$. There are two standard metrics on the Stiefel manifold.

The *Euclidean metric* on T_U is the one inherited from the ambient $\mathbb{R}^{n \times p}$:

$$\langle \Delta, \tilde{\Delta} \rangle_U^e = \text{tr}(\Delta^T \tilde{\Delta}) = \text{tr} A^T \tilde{A} + \text{tr} H^T \tilde{H}.$$

The *canonical metric* on T_U is derived from the quotient representation $St(n, p) = O(n)/(O(n-p))$ of the Stiefel manifold, see [11], and reads

$$\langle \Delta, \tilde{\Delta} \rangle_U^c = \text{tr} \left(\Delta^T \left(I - \frac{1}{2} U U^T \right) \tilde{\Delta} \right) = \frac{1}{2} \text{tr} A^T \tilde{A} + \text{tr} H^T \tilde{H}.$$

Let $A = (a_{ij})_{i,j \leq p}$ and $H = (h_{ij})_{i \leq n; j \leq p}$. The Euclidean metric corresponds to measuring tangent vectors $\Delta = UA + U^\perp H$ in the Frobenius matrix norm

$$\sqrt{\langle \Delta, \Delta \rangle_U^e} = \|\Delta\|_F = \sqrt{\|A\|_F^2 + \|H\|_F^2} = \sqrt{2 \sum_{i < j} a_{ij}^2 + \sum_{i,j} h_{ij}^2},$$

while the canonical metric yields

$$\sqrt{\langle \Delta, \Delta \rangle_U^c} = \sqrt{\frac{1}{2} \|A\|_F^2 + \|H\|_F^2} = \sqrt{\sum_{i < j} a_{ij}^2 + \sum_{i,j} h_{ij}^2}.$$

In this sense, the Euclidean metric disregards the skew-symmetry of A and the independent entries $a_{ij}, i < j$ are counted twice, as was observed in [11, §2.4].

The work [17] recognizes the Euclidean and the canonical metric as special cases of a one-parameter family of inner products

$$(5) \quad \langle \Delta, \tilde{\Delta} \rangle_{\tilde{U}}^{\alpha} = \text{tr} \left(\Delta^T \left(I - \frac{2\alpha + 1}{2(\alpha + 1)} U U^T \right) \tilde{\Delta} \right) = \frac{1}{2(\alpha + 1)} \text{tr} A^T \tilde{A} + \text{tr} H^T \tilde{H},$$

for $\alpha \in \mathbb{R} \setminus \{-1\}$.¹ For $\alpha = -\frac{1}{2}$ and $\alpha = 0$, the Euclidean and the canonical metric are recovered, respectively. As can be seen from (5), the metric parameter α controls how much weight is put on the $\frac{1}{2}(p-1)p$ degrees of freedom in the matrix $A \in \text{skew}(p)$ relative to the $(n-p)p$ degrees of freedom in $H \in \mathbb{R}^{(n-p) \times p}$. Perfect balance is at $\alpha = 0$, which corresponds to the canonical metric.

Calculating the Riemannian Stiefel exponential: The state of the art.

A closed-form expression for the Stiefel exponential w.r.t. the Euclidean metric is derived in [11, §2.2.2],

$$(6) \quad \tilde{U} = \text{Exp}_U^e(\Delta) = \begin{pmatrix} U & \Delta \end{pmatrix} \exp_m \begin{pmatrix} A & -\Delta^T \Delta \\ I_p & A \end{pmatrix} \begin{pmatrix} I_p \\ 0 \end{pmatrix} \exp_m(-A).$$

In [18], an alternative formula is obtained:

$$(7) \quad \tilde{U} = \text{Exp}_U^e(\Delta) = \exp_m(\Delta U^T - U \Delta^T) U \exp_m(-A).$$

The advantage is that in this form, the Stiefel exponential features only matrix exponentials of skew-symmetric matrices. The downside is that $\Delta U^T - U \Delta^T \in \text{skew}(n)$ and working with $(n \times n)$ -matrices might be prohibitively expensive in large-scale applications, where $n \gg p$.

In [17], the formula (7) is generalized to the exponential for all α -metrics of (5),

$$(8) \quad \tilde{U} = \text{Exp}_U^{\alpha}(\Delta) = \exp_m \left(-\frac{2\alpha + 1}{\alpha + 1} U A U^T + \Delta U^T - U \Delta^T \right) U \exp_m \left(\frac{\alpha}{\alpha + 1} A \right).$$

An algorithm for computing the Stiefel exponential w.r.t. the canonical metric was derived in [11, §2.4.2]: Given U, Δ , first compute a compact QR-decomposition $QR = (I - U U^T) \Delta$ with $Q \in St(n, p), R \in \mathbb{R}^{p \times p}$. Then form

$$(9) \quad \tilde{U} = \text{Exp}_U^c(\Delta) = \begin{pmatrix} U & Q \end{pmatrix} \exp_m \begin{pmatrix} A & -R^T \\ R & 0 \end{pmatrix} \begin{pmatrix} I_p \\ 0 \end{pmatrix},$$

where again $A = U^T \Delta \in \text{skew}(p)$. Using this form becomes efficient, if $p < \frac{n}{2}$.

Calculating the Riemannian Stiefel logarithm: State of the art. Computing the Riemannian logarithm corresponds to solving the *geodesic endpoint problem* locally:

Given $U, \tilde{U} \in St(n, p)$ find a starting velocity $\Delta \in T_U$ such that

$$\text{Exp}_U(\Delta) = \tilde{U} \quad \left(\Leftrightarrow \Delta = \text{Log}_U(\tilde{U}) \right).$$

¹For a deeper reason, why $\alpha = -1$ has to be excluded, see [17].

Algorithm 1 Shooting method, adapted from [7, Alg. 1]

Input: Stiefel matrices $U, \tilde{U} \in St(n, p)$, convergence threshold $\epsilon > 0$, time step array

$$T = \{t_0, t_1, \dots, t_m\}, \text{ with } t_0 = 0, t_m = 1.0.$$

- 1: $\gamma \leftarrow \|\tilde{U} - U\|$ {compute gap between base point and target}
- 2: $\Delta \leftarrow \gamma \frac{\Pi_U(\tilde{U})}{\|\Pi_U(\tilde{U})\|}$ {project gap vector $\tilde{U} - U$ onto T_U , preserve length}
- 3: **while** $\gamma > \epsilon$ **do**
- 4: **for** $j = 1, \dots, m$ **do**
- 5: $\tilde{U}^s(j) \leftarrow \text{Exp}_U(t_j \Delta)$ {discrete representation of geodesic}
- 6: **end for**
- 7: $\Delta^s \leftarrow \tilde{U}^s(m) - \tilde{U}$ {current gap vector: compare endpoint of geodesic to \tilde{U} }
- 8: $\gamma \leftarrow \|\Delta^s\|$
- 9: **for** $j = m, \dots, 0$ **do**
- 10: $\Delta^s \leftarrow \gamma \frac{\Pi_{\tilde{U}^s(j)}(\Delta^s)}{\|\Pi_{\tilde{U}^s(j)}(\Delta^s)\|}$ {initial projection plus approximate parallel transport}
- 11: **end for**
- 12: update $\Delta \leftarrow \Delta - \Delta^s$
- 13: **end while**

Output: Δ

Note: The first inner iteration in the loop in steps 9-11 projects the gap vector of step 7 onto $T_{\tilde{U}^s(m)}$. The remaining inner iterations in this loop realize an approximation of the parallel transport along the discretized geodesic $t \mapsto \text{Exp}_U(t\Delta)$.

A generic method for solving the geodesic endpoint problem on any manifold is the shooting method, see [32, section 6.5]. This method is considered in [7] to compute the Stiefel logarithm. For the specific case of $St(4, 2)$ it features in [34]. The generic principle of the shooting method is as follows:

- find an initial guess $\Delta_0 \in T_U$.
- “shoot” a geodesic in the direction of Δ_0 , i.e., compute $\tilde{U}_0 := \text{Exp}_U(\Delta_0)$.
- measure the gap f_g between \tilde{U}_0 and the actual target \tilde{U} as a function of Δ .
- use information on the gap to update $\Delta_1 \leftarrow \Delta_0$ and repeat.

There are many options to implement these steps. In [7], the initial guess is chosen as $\Delta_0 = \Pi_U(U - \tilde{U}) \in T_U$. The gap is measured in the ambient space $\mathbb{R}^{n \times p}$ as $f_g(\Delta) = \|\tilde{U}_0 - \tilde{U}\|_F^2 = \|\text{Exp}_U(\Delta) - \tilde{U}\|_F^2$. A natural choice for updating the shooting direction Δ is a gradient descent based on this gap function. An alternative is to tackle the matrix root finding problem $\text{Exp}_U(\Delta) - \tilde{U} = 0$ with the Newton method. This approach is pursued in [35, Section 2.3]. However, both of these approaches require in particular the derivative of the matrix exponential, which is expensive to obtain, see [15, Section 10.6] for the general formulas and [34, Prop.12], [41, Lem. 5] for precise applications to the Stiefel exponential.

The reference [7] proposes a method that avoids calculating derivatives. The idea is to project the gap vector $\text{Exp}_U(\Delta) - \tilde{U}$ from $\mathbb{R}^{n \times p}$ onto $T_{\tilde{U}}St(n, p)$ and to parallel-translate the result along the geodesic $t \rightarrow \text{Exp}_U(t\Delta)$ back to $T_USt(n, p)$, where the update of the shooting direction Δ is then performed. This process is detailed in [Algorithm 1](#). For a higher computational efficiency, only an approximation of the parallel transport is realized on equidistant time steps $0 = t_0, t_1, \dots, t_m = 1$ in the unit interval $[0, 1]$. The more time steps there are, the more accurate will be the result of the parallel transport. However, this does not help, if the tangent information that

is to be transported is of poor quality in the first place.

The ‘‘multiple shooting’’ as featured in [35, Section 2.4] shares the idea of dissecting the geodesic lines under consideration into m segments. Yet in this method, one actually solves subproblems on the segments with Newton’s method.

A Stiefel log algorithm that is tailored for the canonical metric and features guaranteed local linear convergence is given in [40]. This approach will be explained and enhanced in [Subsection 3.4](#).

3. Fast computational schemes for solving the geodesic endpoint problem. In this section, we first prepare the grounds for a unified framework to tackle the local geodesic endpoint problem on the Stiefel manifold under the one-parameter family of metrics. Then, we introduce practical numerical algorithms for computing the associated Stiefel logarithm, which improve on the state of the art in terms of the computational efficiency.

3.1. A reduced formula for the Stiefel exponential. As a starting point for efficient computational schemes, we derive an alternative expression for the α -metric Stiefel exponential that combines the advantages of (6) and (8) and represents a considerable computational reduction if $n \gg p$. To this end, assume that $p \leq \frac{n}{2}$. Let $U \in St(n, p)$ be given and take any suitable column-orthonormal extension $U^\perp \in St(n - p, p)$, i.e., any U^\perp such that $\Phi = (U \mid U^\perp) \in O(n)$ is square and orthogonal.

Observe that $\Phi^T U = \begin{pmatrix} I_p \\ 0 \end{pmatrix}$. With $\nu = \frac{2\alpha+1}{\alpha+1}$, $\mu = \frac{\alpha}{\alpha+1} = \nu - 1$, we rewrite (8):

$$\begin{aligned}
 \text{Exp}_U^\alpha(\Delta) &= \Phi \Phi^T \exp_m(-\nu U A U^T + \Delta U^T - U \Delta^T) \Phi \Phi^T U \exp_m(\mu A) \\
 &= \Phi \exp_m(-\nu \Phi^T U A U^T \Phi + \Phi^T (\Delta U^T - U \Delta^T) \Phi) \Phi^T U \exp_m(\mu A) \\
 &= \Phi \exp_m \begin{pmatrix} -\nu A + U^T \Delta - \Delta^T U & -\Delta^T U^\perp \\ (U^\perp)^T \Delta & 0 \end{pmatrix} \begin{pmatrix} I_p \\ 0 \end{pmatrix} \exp_m(\mu A) \\
 (10) \quad &= (U \mid U^\perp) \exp_m \begin{pmatrix} (2-\nu)A & -H^T \\ H & 0 \end{pmatrix} \begin{pmatrix} I \\ 0 \end{pmatrix} \exp_m(\mu A), \quad H = (U^\perp)^T \Delta.
 \end{aligned}$$

Let $H = \tilde{Q} \begin{pmatrix} B \\ 0 \end{pmatrix}$ with $\tilde{Q} = (\tilde{Q}_p \mid \tilde{Q}_{n-2p}) \in O(n-p)$ be a (full) QR-decomposition of H . (Only the orthonormality of \tilde{Q} matters, B need not be triangular for the following considerations.) We can factor

$$\begin{pmatrix} (2-\nu)A & -H^T \\ H & 0 \end{pmatrix} = \begin{pmatrix} I_p & 0 \\ 0 & \tilde{Q} \end{pmatrix} \exp_m \begin{pmatrix} (2-\nu)A & -B^T & 0 \\ B & 0 & 0 \\ 0 & 0 & 0 \end{pmatrix} \begin{pmatrix} I_p & 0 \\ 0 & \tilde{Q}^T \end{pmatrix},$$

which yields $\text{Exp}_U^\alpha(\Delta) = (U \mid U^\perp \tilde{Q}_p) \exp_m \begin{pmatrix} (2-\nu)A & -B^T \\ B & 0 \end{pmatrix} \begin{pmatrix} \exp_m(\mu A) \\ 0 \end{pmatrix}$. Note that $U^\perp H = U^\perp (U^\perp)^T \Delta = (I - U U^T) \Delta$. Hence, instead of computing a QR-decomposition of $U^\perp H$, we can directly compute a compact QR-decomposition $(I - U U^T) \Delta = Q B$ with $Q \in St(n, p)$ (Again, no special structure is required for $B \in \mathbb{R}^{p \times p}$.) This leads to the following proposition.

PROPOSITION 1. *Let $\alpha \neq -1$. For $U \in St(n, p)$, $\Delta \in T_U St(n, p)$ the Stiefel exponential under the α -metric of (5) reads*

$$(11) \quad \text{Exp}_U^\alpha(\Delta) = (U \mid Q) \exp_m \begin{pmatrix} \frac{1}{\alpha+1} A & -B^T \\ B & 0 \end{pmatrix} \begin{pmatrix} I_p \\ 0 \end{pmatrix} \exp_m \left(\frac{\alpha}{\alpha+1} A \right),$$

where $A = U^T \Delta \in \text{skew}(p)$ and $QB = (I - UU^T)\Delta \in \mathbb{R}^{n \times p}$ is any matrix decomposition with $Q \in St(n, p)$ and $B \in \mathbb{R}^{p \times p}$.

As with (9), this form features only standard matrix exponentials of skew-symmetric matrices of size p rather than n . With [Proposition 1](#), the Stiefel exponential is computable for all metrics in the α -family (5) in $\mathcal{O}(np^2)$ flops. A more detailed look on the calculations reveals that the formula (11) remains valid also if $p > \frac{n}{2}$. However, in this case, it represents in fact an increase in dimension for the main matrix exponential rather than a reduction when compared to (8). The formula (11) continues to hold if the orthogonal component $(I - UU^T)\Delta$ of the tangent vector is rank-deficient. In this case, it is understood that the QR-decomposition $QB = (I - UU^T)\Delta$ be arranged such that $QB = (Q_r \mid Q_{p-r}) \begin{pmatrix} B_r \\ 0 \end{pmatrix}$, where $B_r \in \mathbb{R}^{r \times p}$ and $\text{rank}(B_r) = \text{rank}((I - UU^T)\Delta) = r$ and $B_r = 0$ in the extreme case of $0 = (I - UU^T)\Delta$.

Before we continue with the main body of this work, we note an interesting aside.

LEMMA 2. For $A \in \text{skew}(p)$, $H \in \mathbb{R}^{(n-p) \times p}$, it holds

$$\begin{pmatrix} I_p & A \\ 0 & H \end{pmatrix} \exp_m \begin{pmatrix} A & A^2 - H^T H \\ I_p & A \end{pmatrix} \begin{pmatrix} I_p \\ 0 \end{pmatrix} = \exp_m \begin{pmatrix} 2A & -H^T \\ H & 0 \end{pmatrix} \begin{pmatrix} I_p \\ 0 \end{pmatrix}.$$

Proof. Fix an orthogonal matrix $(U \mid U^\perp) \in O(n)$ and construct $\Delta = UA + U^\perp H$. Then, the lemma is a consequence of the fact that both (6) and (10) with $\alpha = -\frac{1}{2}$ are valid expressions of the (unique) Stiefel matrix exponential $\text{Exp}_U^\epsilon(\Delta)$. The underlying geodesics $t \mapsto \text{Exp}_U^\epsilon(t\Delta)$ satisfy the same initial value problem and thus coincide, see [20, Theorem 4.27, p. 103]. \square

3.2. The Stiefel log matrix equations. We continue to work under the assumption that $p \leq \frac{n}{2}$ with the setting of $n \gg p$ in mind for practical big-data applications. In this section, we show that, in essence, computing the Stiefel logarithm for all α -metrics corresponds to solving a nonlinear matrix equation, where the unknown is a $2p \times 2p$ skew-symmetric matrix.

Let $U \in St(n, p)$ and let $\tilde{U} \in St(n, p)$ be within the injectivity radius $r_{St}(U)$ of $St(n, p)$ at U . Let $\Delta \in T_U$ be such that $\text{Exp}_U^\alpha(\Delta) = \tilde{U}$. Then, \tilde{U} has a representation

$$\tilde{U} = UM + QN, \quad M, N \in \mathbb{R}^{n \times p}, \quad M^T M + N^T N = I_p,$$

where $Q \in St(n, p)$ is the ‘ Q -factor’ of a compact QR-decomposition $QB = (I - UU^T)\Delta$. For the canonical metric ($\alpha = 0$), this is immediately clear from (9). For the full family of α -metrics, this follows from (11). More precisely, M, N form the first block column of an orthogonal matrix

$$(12) \quad \begin{pmatrix} M & X \\ N & Y \end{pmatrix} = \exp_m \begin{pmatrix} \frac{1}{\alpha+1}A & -B^T \\ B & 0 \end{pmatrix} \begin{pmatrix} \exp_m(\frac{\alpha}{\alpha+1}A) & 0 \\ 0 & I_p \end{pmatrix} \in SO(2p).$$

Recall $A = U^T \Delta \in \text{skew}(p)$ and that $\alpha = 0$ and $\alpha = -\frac{1}{2}$ reproduce the canonical and the Euclidean metric, respectively. For brevity, write again

$$\mu = \frac{\alpha}{\alpha+1}, \quad \alpha \neq -1.$$

Now, we aim at finding the inverse $(\text{Exp}_U^\alpha)^{-1}(\tilde{U}) = \Delta$ with Δ as unknown. We can still obtain M and N from the given data points U, \tilde{U} via

$$M = U^T \tilde{U}, \quad QN = (I - UU^T)\tilde{U}.$$

For the latter equation, any matrix decomposition that represents $(I - UU^T)\tilde{U}$ via a ‘subspace factor’ Q with orthonormal columns and a corresponding ‘coordinates factor’ N is suitable in order to obey the constraint that M and N be blocks of an orthogonal matrix, i.e., $I = M^T M + N^T N$. This incorporates some ambiguity. If $(I - UU^T)\tilde{U}$ has full rank p , then Q and N are unique up to a rotation/reflection $\Phi \in O(p)$. More precisely, for $\tilde{Q}\tilde{N} = (I - UU^T)\tilde{U} = QN$, it holds $Q = \tilde{Q}\Phi, N = \Phi^T\tilde{N}$ with $\Phi = \tilde{Q}^T Q$. If $\text{rank}(I - UU^T)\tilde{U} = r < p$, then we may assume that

$$(13) \quad (I - UU^T)\tilde{U} = QN = (Q_r \mid Q_{p-r}) \begin{pmatrix} N_r \\ 0 \end{pmatrix},$$

where $Q_r \in St(n, r), Q_{p-r} \in St(n, p-r), N_r \in \mathbb{R}^{p \times r}$. This determines Q_r, N_r uniquely up to a rotation/reflection $\Phi_r \in O(r)$. Yet, the column block Q_{p-r} may be an arbitrary orthonormal extension.

Once Q, M, N are chosen and fixed, we can compute matrix blocks X_0, Y_0 such that they form an orthogonal completion $V = \begin{pmatrix} M & X_0 \\ N & Y_0 \end{pmatrix} \in O(2p)$. The restriction of the exponential map to the skew-symmetric matrices

$$\exp_m|_{\text{skew}(p)} : \text{skew}(p) \rightarrow SO(p)$$

is surjective [13, §. 3.11, Thm. 9]. Hence, (12) requires to select X_0, Y_0 such that $\det(V) = +1$.² Again, such a completion is not unique and it cannot be expected that the such found X_0, Y_0 align with the structure of (12). Yet, there is an orientation preserving orthogonal matrix $\Phi = \exp_m(C), C \in \text{skew}(p)$ such that $\begin{pmatrix} X_0 \\ Y_0 \end{pmatrix} \Phi = \begin{pmatrix} X \\ Y \end{pmatrix}$ is the sought-after completion. In summary, computing the Stiefel logarithm boils down to solving the following nonlinear matrix equation:

$$(14) \quad \text{solve } F \begin{pmatrix} A & -B^T \\ B & C \end{pmatrix} = \begin{pmatrix} M & X_0 \\ N & Y_0 \end{pmatrix}, \quad \text{for } F : \text{skew}(2p) \rightarrow SO(2p),$$

$$F \begin{pmatrix} A & -B^T \\ B & C \end{pmatrix} = \exp_m \begin{pmatrix} (1 - \mu)A & -B^T \\ B & 0 \end{pmatrix} \begin{pmatrix} \exp_m(\mu A) & 0 \\ 0 & \exp_m(-C) \end{pmatrix}, \mu = \frac{\alpha}{\alpha + 1}.$$

The sought-after tangent vector is then $\Delta = UA + QB \in T_U$. It is worth mentioning that any ambiguity in Q has no impact on the final Δ , not even in the case where the component $(I - UU^T)\tilde{U}$ of \tilde{U} does not feature full rank. This is confirmed in the next theorem, which can be considered as a generalization of [40, Thm. 3.1].

THEOREM 3. *Let $U, \tilde{U} \in St(n, p)$ with $\text{dist}(U, \tilde{U}) < r_{St}(U)$ and let*

$$U^T \tilde{U} = M, \quad (I - UU^T)\tilde{U} = QN = (Q_r \mid Q_{p-r}) \begin{pmatrix} N_r \\ 0 \end{pmatrix}, \quad r \leq p,$$

with $Q \in St(n, p)$ and $r = \text{rank}(N_r) = \text{rank}(N)$. Then $\Delta = \text{Log}_U^\alpha(\tilde{U})$ features a representation

$$\Delta = UA + QB = UA + (Q_r \mid Q_{p-r}) \begin{pmatrix} B_r \\ 0 \end{pmatrix}, \quad A \in \text{skew}(p), \quad B_r \in \mathbb{R}^{r \times p}.$$

Here, A, B are components of a skew-symmetric block matrix that solves (14).

²As an aside, this is why the example S1 from the supplements of [40] fails.

Proof. Let $M, N \in \mathbb{R}^{p \times p}$, with $N = \begin{pmatrix} N_r \\ 0 \end{pmatrix}$, $N_r \in \mathbb{R}^{r \times p}$ of full rank r constructed as stated above. We can restrict the considerations to block extensions X_0, Y_0 to an orthogonal matrix of the form

$$V = \begin{pmatrix} M & X_0 \\ N & Y_0 \end{pmatrix} = \left(\begin{array}{c|c|c} M & X_r^0 & 0 \\ \hline N_r & Y_r^0 & 0 \\ \hline 0 & 0 & I_{p-r} \end{array} \right) \in SO(2p),$$

where $X_r^0 \in \mathbb{R}^{p \times r}$, $Y_r^0 \in \mathbb{R}^{r \times r}$ are obtained, say, via the Gram-Schmidt method.

Let $\begin{pmatrix} A & -B^T \\ B & C \end{pmatrix}$ be a solution to (14) that preserves the above structure of V so that

in particular $\begin{pmatrix} X_r^0 & 0 \\ Y_r^0 & 0 \\ 0 & I_{p-r} \end{pmatrix} \exp_m(C) = \begin{pmatrix} X_r & 0 \\ Y_r & 0 \\ 0 & I_{p-r} \end{pmatrix}$. This entails $\exp_m(C) = \Phi =$

$\begin{pmatrix} \Phi_r & 0 \\ 0 & I_{p-r} \end{pmatrix} \in SO(p)$. Then, for all α -metrics, it holds with $\mu = \frac{\alpha}{\alpha+1}$ that

$$(15) \quad \log_m \left(\begin{pmatrix} M & X_r^0 & 0 \\ N_r & Y_r^0 & 0 \\ 0 & 0 & I_{p-r} \end{pmatrix} \begin{pmatrix} \exp_m(-\mu A) & 0 & 0 \\ 0 & \Phi_r & 0 \\ 0 & 0 & I_{p-r} \end{pmatrix} \right) = \begin{pmatrix} (1-\mu)A & -B^T \\ B & 0 \end{pmatrix}.$$

Because the matrix logarithm acts block-wise on block-diagonal matrices, the block structure of the matrix on the left hand side entails a corresponding block structure for the right-hand side of (15). In particular, necessarily $B = \begin{pmatrix} B_r \\ 0 \end{pmatrix}$ with $\text{rank}(B_r) = r$.

Now, define $\Delta = UA + Q_r B_r$ and evaluate the Stiefel exponential to check if $\text{Exp}_U^\alpha(\Delta) = \tilde{U}$. According to (11), the procedure requires to compute $U^T \Delta = A$, as well as an orthogonal decomposition

$$(I - UU^T)\Delta = \begin{pmatrix} \hat{Q}_r & \hat{Q}_{p-r} \end{pmatrix} \begin{pmatrix} \hat{B}_r \\ 0 \end{pmatrix}.$$

The matrix factors \hat{Q}_r and \hat{B}_r are not necessarily equal to Q_r and B_r , respectively. Yet, by construction, it holds $\hat{Q}_r \hat{B}_r = (I - UU^T)\Delta = (I - UU^T)Q_r B_r = Q_r B_r$. Since Q_r, \hat{Q}_r span the same column-space, $S := Q_r^T \hat{Q}_r$ is orthogonal and $\hat{Q}_r = Q_r S, \hat{B}_r = S^T B_r$. The Stiefel exponential produces

$$\begin{aligned} \text{Exp}_U^\alpha(\Delta) &= \left(U \mid \hat{Q}_r \mid \hat{Q}_{p-r} \right) \exp_m \begin{pmatrix} (1-\mu)A & -\hat{B}_r^T & 0 \\ \hat{B}_r & 0 & 0 \\ 0 & 0 & 0 \end{pmatrix} \begin{pmatrix} \exp_m(\mu A) \\ 0 \\ 0 \end{pmatrix} \\ &= \left(U \mid \hat{Q}_r \right) \exp_m \begin{pmatrix} (1-\mu)A & -\hat{B}_r^T \\ \hat{B}_r & 0 \end{pmatrix} \begin{pmatrix} \exp_m(\mu A) \\ 0 \end{pmatrix} \\ &= \left(U \mid \hat{Q}_r S \right) \exp_m \begin{pmatrix} (1-\mu)A & -\hat{B}_r^T S \\ S^T \hat{B}_r & 0 \end{pmatrix} \begin{pmatrix} \exp_m(\mu A) \\ 0 \end{pmatrix} \\ &= \left(U \mid Q_r \right) \exp_m \begin{pmatrix} (1-\mu)A & -B_r^T \\ B_r & 0 \end{pmatrix} \begin{pmatrix} \exp_m(\mu A) \\ 0 \end{pmatrix} = \left(U \mid Q_r \right) \begin{pmatrix} M \\ N_r \end{pmatrix} = \tilde{U} \end{aligned}$$

according to (15). \square

Remark 4 (The search space for the Stiefel log algorithm). For Stiefel points U and $\tilde{U} = \text{Exp}_U^\alpha(\Delta)$ within the injectivity radius at U , [Theorem 3](#) shows that both the location \tilde{U} and the tangent vector Δ are in the same matrix space

$$(16) \quad \mathcal{S} = \{UV | V \in \mathbb{R}^{p \times p}\} \oplus \{QW | W \in \mathbb{R}^{p \times p}\} \subset \mathbb{R}^{n \times p}.$$

This fact can be exploited in numerical schemes for computing the Stiefel logarithm. A direct consequence is that any numerical algorithm can focus on finding the missing factors $A, B \in \mathbb{R}^{p \times p}$.

3.3. A p -shooting method tailored to the Stiefel logarithm. In this section, we customize the generic iterative shooting method of [Algorithm 1](#) for solving the geodesic endpoint problem. With large “tall-and-skinny” matrices and big data applications in mind, our contribution is to modify the required calculations such that the loop iterations are tailored for the use of (11) and (16) and work exclusively with $2p \times 2p$ matrices rather than with $n \times p$ matrices. This leads to considerable savings, if $n \gg p$.

Given $U, \tilde{U} \in St(n, p)$, the starting point is the representation $\tilde{U} = UU^T\tilde{U} + (I - UU^T)\tilde{U} = U\widehat{M} + Q\widehat{N}$, where $\widehat{M} = U^T\tilde{U} \in \mathbb{R}^{p \times p}$ and $Q\widehat{N} = (I - UU^T)\tilde{U} \in \mathbb{R}^{n \times p}$ is a compact QR-decomposition. The essential observation is that all iterates Δ, Δ^s of [Algorithm 1](#) actually remain in the matrix space \mathcal{S} of (16) that is spanned by the fixed U and Q . According to [Theorem 3](#) and [Remark 4](#), \mathcal{S} also contains the sought-after solution.

PROPOSITION 5. *Let $U, \tilde{U} \in St(n, p)$ and let $Q\widehat{N} = (I - UU^T)\tilde{U} \in \mathbb{R}^{n \times p}$ be a compact QR-decomposition. All tangent matrices Δ produced iteratively by [Algorithm 1](#) and all the update matrices Δ^s that are the final outcome of one pass through the while-loop in [Algorithm 1](#) allow for a representation of the form*

$$\Delta = UA + QR, \quad \Delta^s = UA^s + QR^s, \quad A, A^s \in \text{skew}(p), R, R^s \in \mathbb{R}^{p \times p}.$$

Remark: It is important to emphasize that it is *the same* Q-factor that works for all the iterates Δ, Δ^s . This enables to restrict the update to the A- and R-factors. The intermediate matrices Δ^s under the while-loop are also contained in the matrix space \mathcal{S} of [Remark 4](#), but they are of the form $\Delta^s = UX^s + QR^s$ with $X^s \notin \text{skew}(p)$ in general.

Proof. The initial Δ_0 is obtained from the projection

$$\begin{aligned} \Delta_0 &= \Pi_U(\tilde{U} - U) = \Pi_U(\tilde{U}) = U\widehat{M} + Q\widehat{N} - U \text{sym}(\widehat{M}) \\ &= U \text{skew}(\widehat{M}) + Q\widehat{N} =: UA_0 + QR_0. \end{aligned}$$

The first update Δ^s is obtained by projecting the gap vector $\tilde{U}_0^s - U$ onto $T_{\tilde{U}}$ and then further onto T_U by following the geodesic ‘backwards in time’, see steps 9–11 in [Algorithm 1](#). At every time instant t , it holds

$$\tilde{U}^s(t) = \text{Exp}_U^\alpha(t\Delta_0) = (U \mid Q) \begin{pmatrix} M_t & X_t \\ N_t & Y_t \end{pmatrix} \begin{pmatrix} I_p \\ 0 \end{pmatrix} = UM_t + QN_t,$$

where $\begin{pmatrix} M_t & X_t \\ N_t & Y_t \end{pmatrix}$ is evaluated according to (12) with inputs $A = tA_0, B = tR_0$.

If any matrix of the form $W = UX + QY$ is projected onto the tangent space at any $UM_t + QN_t$, the result is

$$\begin{aligned} \Pi_{UM_t + QN_t}(W) &= U(X - M_t \text{sym}(M_t^T X + N_t^T Y)) + Q(Y - N_t \text{sym}(M_t^T X + N_t^T Y)) \\ &= UX^\Pi + QY^\Pi. \end{aligned}$$

Hence, all operations performed in [Algorithm 1](#) take place in the matrix space $\mathcal{S} = \{UX + QY | X, Y \in \mathbb{R}^{p \times p}\}$ of (16). \square

With [Proposition 5](#), the computational costs associated with the shooting method can be reduced considerably. This gives rise to [Algorithm 2](#). A few remarks on this

Algorithm 2 p-Shooting method

Input: Stiefel matrices $U, \tilde{U} \in St(n, p)$, convergence threshold $\epsilon > 0$, array $T = [t_0, t_1, \dots, t_m]$, $t_0 = 0, t_m = 1.0$ (discretized unit interval), metric parameter α .

- 1: $\widehat{M} = U^T \tilde{U}$
 - 2: $Q\widehat{N} = \tilde{U} - U\widehat{M}$ {compact QR-decomposition}
 - 3: $\gamma \leftarrow \sqrt{\|\widehat{M} - I_p\|^2 + \|\widehat{N}\|^2}$ {note $\tilde{U} - U = U(\widehat{M} - I_p) + Q\widehat{N}$ }
 - 4: $A \leftarrow \frac{\gamma \text{skew}(\widehat{M})}{\sqrt{\|\text{skew}(\widehat{M})\|^2 + \|\widehat{N}\|^2}}, \quad R \leftarrow \frac{\gamma \widehat{N}}{\sqrt{\|\text{skew}(\widehat{M})\|^2 + \|\widehat{N}\|^2}},$
 - 5:
 - 6: **while** $\gamma > \epsilon$ **do**
 - 7: **for** $j = 1, \dots, m$ **do**
 - 8: $\begin{pmatrix} M(t_j) \\ N(t_j) \end{pmatrix} \leftarrow \exp_m \left(t_j \begin{pmatrix} \frac{1}{\alpha+1} A & -R^T \\ R & 0 \end{pmatrix} \right) \begin{pmatrix} \exp_m \left(t_j \begin{pmatrix} \alpha \\ \alpha+1 \end{pmatrix} A \right) \\ 0 \end{pmatrix}$ {cf. (12)}
 - 9: **end for** {p-factor representation of geodesic $U^s(t_j) = UM(t_j) + QN(t_j)$ }
 - 10: $A^s \leftarrow M(t_m) - \widehat{M}, R^s \leftarrow N(t_m) - \widehat{N}$ {p-factors of current gap vector}
 - 11: $\gamma \leftarrow \sqrt{\|A^s\|^2 + \|R^s\|^2}$
 - 12: **for** $j = m, \dots, 0$ **do**
 - 13: $[A^s, R^s] = \text{ParaTrans_pFactors}(M(t_j), N(t_j), A^s, R^s, \gamma)$ {initial projection
plus approximate parallel transport}
 - 14: **end for**
 - 15: update $A \leftarrow A - A^s, \quad R \leftarrow R - R^s$ {updated $\Delta = UA + QR$ }
 - 16: **end while**
- Output:** $\Delta = UA + QR$
-

procedure are in order: Observe that step 8 of [Algorithm 2](#) is the only step that depends on the chosen metric and thus makes the only difference when computing the Stiefel logarithm for the canonical, the Euclidean or any other α -metric. The subroutine $\text{ParaTrans_pFactors}(M(t), N(t), A^s, R^s, \gamma)$ that appears in step 13 of [Algorithm 2](#) realizes an approximation of the parallel transport of $\Delta^s = UA^s + QR^s$ along the geodesic using the unique representation with the p -factors A^s, R^s . This subroutine is detailed in [Algorithm 3](#). A numerical experiment that illustrates the performance of [Algorithm 2](#) is given in [Section 4](#).

3.4. An improved algebraic Stiefel logarithm for the canonical metric.

Let $U, \tilde{U} = UM + QN \in St(n, p)$ with $M = U^T \tilde{U}, QN = (I - UU^T)\tilde{U}$ and an orthonormal completion $\begin{pmatrix} M & X_0 \\ N & Y_0 \end{pmatrix} \in SO(2p)$ as introduced in the previous sections. In [\[40\]](#), it has been shown that for solving [\(14\)](#) in the case of the canonical metric, it

Algorithm 3 ParaTrans_pFactors: Map the tangent vector $\Delta = UA_1 + QR_1 \in T_{U_1}$ to the tangent space T_{U_2} , preserve the length

Input: $M_2, N_2, A_1, R_1 \in \mathbb{R}^{p \times p}$, $\gamma > 0$

{here, M_2, N_2 represent $U_2 = UM_2 + QN_2 \in St(n, p)$, A_1, R_1 represent $\Delta = UA_1 + QR_1 \in T_{U_1}$.}

- 1: $S \leftarrow \text{sym}(M_2^T A_1 + N_2^T R_1)$
- 2: $A_2 = A_1 - M_2 S$, $R_2 = R_1 - N_2 S$
- 3: $l = \sqrt{\|A_2\|^2 + \|R_2\|^2}$
- 4: **if** $l > \epsilon$ **then**
- 5: $A_2 = \frac{\gamma}{l} A_2$, $R_2 = \frac{\gamma}{l} R_2$ {rescale to original length}
- 6: **else**
- 7: $A_2 = 0$, $R_2 = 0$.
- 8: **end if**

Output: A_2, R_2

This algorithm executes the same operation as in step 10 of [Algorithm 1](#) but on the representative $p \times p$ matrix factors.

is sufficient to find $\Gamma \in \text{skew}(p)$ such that

$$(17) \quad (0 \mid I_p) \log_m \left(\begin{pmatrix} M & X_0 \\ N & Y_0 \end{pmatrix} \begin{pmatrix} I_p & 0 \\ 0 & \exp_m(\Gamma) \end{pmatrix} \right) \begin{pmatrix} 0 \\ I_p \end{pmatrix} = 0 \in \mathbb{R}^{p \times p}.$$

With $V = \begin{pmatrix} M & X_0 \\ N & Y_0 \end{pmatrix} = \exp_m \begin{pmatrix} A_0 & -B_0^T \\ B_0 & C_0 \end{pmatrix}$ and $W = \exp_m \begin{pmatrix} 0 & 0 \\ 0 & \Gamma \end{pmatrix}$, (17) requires to find Γ such that the lower p -by- p diagonal block of the matrix $\log_m(VW)$ vanishes. Let $[V, W] = VW - WV$ denote the matrix commutator. The Baker-Campbell-Hausdorff (BCH) series for the matrix logarithm is

$$\begin{aligned} \log_m(VW) &= \log_m(V) + \log_m(W) + \frac{1}{2}[\log_m(V), \log_m(W)] \\ &+ \frac{1}{12}([\log_m(V), [\log_m(V), \log_m(W)]] + [\log_m(W), [\log_m(W), \log_m(V)]]) + \dots, \end{aligned}$$

see [30, §1.3, p. 22]. The algorithm [40, Alg. 1] and the associated convergence analysis rely on the fact that with the choice of $\Gamma_0 = -C_0$, the lower p -by- p block of $\log_m(VW)$ vanishes up to terms of third order in the BCH series. The algorithm iterates on this observation and produces the sequence

$$(18) \quad \begin{pmatrix} A_{k+1} & -B_{k+1}^T \\ B_{k+1} & C_{k+1} \end{pmatrix} := \log_m \left(\exp_m \begin{pmatrix} A_k & -B_k^T \\ B_k & C_k \end{pmatrix} \exp_m \begin{pmatrix} 0 & 0 \\ 0 & \Gamma_k \end{pmatrix} \right),$$

with $\Gamma_k = -C_k$. It is guaranteed that $\|C_k\| \rightarrow 0$ for $k \rightarrow \infty$ at a linear rate as long as the input points U, \tilde{U} are close enough, see [40, Theorem 4.1].

In fact, up to commutator products of order three or higher, the BCH series expansion of the lower diagonal block of $\log_m(V_k W)$ is

$$\begin{aligned} &C_k + \Gamma + \frac{1}{2}(C_k \Gamma - \Gamma C_k) \\ &+ \frac{1}{12}(C_k^2 \Gamma + \Gamma C_k^2 + C_k \Gamma^2 + \Gamma^2 C_k - (B_k B_k^T \Gamma + \Gamma B_k B_k^T) - 2(C_k \Gamma C_k + \Gamma C_k \Gamma)) \\ &= C_k + \Gamma + \frac{1}{2}(C_k \Gamma - \Gamma C_k) - \frac{1}{12}(B_k B_k^T \Gamma + \Gamma B_k B_k^T) + \text{h.o.t.} \end{aligned}$$

where “h.o.t.” comprises the higher-order terms in the BCH series. Ignoring the quadratic terms $\Gamma C_k, C_k \Gamma$ and the higher ones and setting the above expression to zero yields a symmetric Sylvester equation for Γ :

$$(19) \quad C_k = S_k \Gamma + \Gamma S_k, \quad \text{with } S_k := \left(\frac{1}{12} B_k B_k^T - \frac{1}{2} I_p \right).$$

A sufficient criterion that guarantees a unique solution is that $\|B_k\|_2 < \sqrt{6}$, since in this case $\frac{1}{6} \|B_k B_k^T\|_2 < 1$, which entails that all eigenvalues of S_k are strictly negative. This in turn yields that S_k and $-S_k$ have disjoint spectra, which ensures the unique solvability of (19), [6, Section VII.2]. When selecting Γ_k as the solution to (19) at each iteration k , then the lower p -by- p diagonal block of the BCH series vanishes up to fourth order commutator terms and terms that are quadratic in C_k and Γ_k . This idea was first presented in [42].

Remark 6. This choice does not cancel all terms that are of first order in Γ in the BCH series of $\log_m(VW)$. The series is ordered by the degree of nested commutator brackets. In the j th-order commutator term, “words” formed by j “letters” of the two-letter alphabet $\{\log_m(V), \log_m(W)\}$ appear, where each of $\log_m(V), \log_m(W)$ appears at least once, see [37, 24, 39]. This means that no matter where we cut off the tail of the BCH series, there remain terms that are linear in $\|\Gamma\|$ (or $\|C_k\|$ for that matter). Expanding this series for $\log_m(VW)$ in powers of W as in [23, Section 8.1] will not solve the issue, because the collection of all terms that are of first order in $\|W\|$ constitutes an infinite series by itself that needs to be truncated in numerical applications.

In the numerical implementation of Algorithm 4, we introduce a Boolean “Flag_Sylv on/off” to switch between the original version [40, Alg. 1], which works with $\Gamma_k = -C_k$ and the “Sylvester-enhancement”, which selects Γ_k as the solution to (19). A detailed convergence analysis can be conducted as in [40] but is not worthwhile in the context of this work. Yet, the next proposition allows to compare the asymptotic convergence rate of Algorithm 4 with “Flag_Sylv” switched off, which is [40, Alg. 1] and Algorithm 4 with “Flag_Sylv” switched on, which is based on solving (19).

PROPOSITION 7. *Suppose that the input data $U \neq \tilde{U} \in St(n, p)$ are such that Algorithm 4 converges with “Flag_Sylv” switched on. Assume further that there is a bound $0 < \delta < 1$ such that for $\log_m(V_k) = \begin{pmatrix} A_k & -B_k^T \\ B_k & C_k \end{pmatrix}$, it holds $\|\log_m(V_k)\|_2 < \delta$ throughout the algorithm’s iteration loop.³ Then, for k large enough, it holds*

$$\|C_{k+1}\|_2 \leq \left(\frac{6}{6 - \delta^2} \frac{\delta^4}{1 - \delta} + \mathcal{O}(\|C_k\|_2) \right) \|C_k\|_2.$$

This implies the asymptotic convergence rate of Algorithm 4 with “Flag_Sylv” switched on for $k \rightarrow \infty$. This compares to the asymptotic rate of [40, Alg. 1], which according to [40, eq. (12)] is bounded by

$$\|C_{k+1}\|_2 \leq \left(\frac{1}{6} \delta^2 + \frac{\delta^4}{1 - \delta} + \mathcal{O}(\|C_k\|_2) \right) \|C_k\|_2.$$

³For the original Stiefel log algorithm, conditions for the existence of such a global bound δ are established in [40, Lemma 4.4]. Similar techniques apply in the present context.

Algorithm 4 Improved algebraic Stiefel logarithm, canonical metric ($\alpha = 0$).

Input: $U, \tilde{U} \in St(n, p)$, $\epsilon > 0$ convergence threshold, Boolean “Flag_Sylv on/off”

- 1: $M := U^T \tilde{U} \in \mathbb{R}^{p \times p}$
- 2: $QN := \tilde{U} - UM \in \mathbb{R}^{n \times p}$ {compact QR-decomp.}
- 3: $V_0 := \begin{pmatrix} M & X_0 \\ N & Y_0 \end{pmatrix} \in O_{2p \times 2p}$ {orthonormal completion}
- 4: **for** $k = 0, 1, 2, \dots$ **do**
- 5: $\begin{pmatrix} A_k & -B_k^T \\ B_k & C_k \end{pmatrix} := \log_m(V_k)$ {matrix log, A_k, C_k skew}
- 6: **if** $\|C_k\|_2 \leq \epsilon$ **then**
- 7: **break**
- 8: **end if**
- 9: **if** Flag_Sylv **then**
- 10: $S_k := \frac{1}{12} B_k B_k^T - \frac{1}{2} I_p$
- 11: solve $C_k = S_k \Gamma + \Gamma S_k$ for Γ {sym. Sylvester equation}
- 12: **else**
- 13: $\Gamma := -C_k$ {cancel first term in BCH series}
- 14: **end if**
- 15: $\Phi_k := \exp_m(\Gamma)$ {matrix exp, Φ_k orthogonal}
- 16: $V_{k+1} := V_k W_k$, where $W_k := \begin{pmatrix} I_p & 0 \\ 0 & \Phi_k \end{pmatrix}$ {update}
- 17: **end for**

Output: $\Delta := \text{Log}_U^{St}(\tilde{U}) = UA_k + QB_k \in T_U St(n, p)$

Proof. Since $\|B_k\|_2 \leq \|\log_m(V_k)\| < \delta < 1$, the matrices $S_k = \frac{1}{12} B_k B_k^T - \frac{1}{2} I_p$ are negative definite with largest eigenvalue bounded by $-\frac{1}{2} + \frac{\delta^2}{12} = -\frac{6-\delta^2}{12}$. Hence, the spectra of the symmetric matrices S_k and $-S_k$ are separated by a vertical strip of width $\frac{6-\delta^2}{6}$ in the complex plain. Applying [6, Theorem VII.2.12] to the Sylvester equation $S_k \Gamma + \Gamma(-S_k) = C_k$ yields $\|\Gamma\|_2 \leq \frac{6}{6-\delta^2} \|C_k\|_2$. Calculating C_{k+1} according to (18) but with this choice of Γ shows that all terms up to order four in the BCH series are at least quadratic in $\|C_k\|_2$:

$$\begin{aligned} C_{k+1} &= \frac{1}{2}[C_k, \Gamma] + \frac{1}{12}([C_k^2, \Gamma] + [C_k, \Gamma^2]) - 2(C_k \Gamma C_k + \Gamma C_k \Gamma) \\ &\quad + \frac{1}{24}([B_k B_k^T, \Gamma^2] - (C_k^2 \Gamma^2 + \Gamma^2 C_k^2) + 2[C_k \Gamma C_k, \Gamma]) + \text{h.o.t.}(5), \end{aligned}$$

where h.o.t.(5) are the terms of fifth order and higher in the BCH series. From $U \neq \tilde{U}$, we get $\lim_{k \rightarrow \infty} \begin{pmatrix} A_k & -B_k^T \\ B_k & C_k \end{pmatrix} \neq 0$. Hence, for k large enough, it holds $\|\Gamma\|_2 \leq \frac{6}{6-\delta^2} \|C_k\|_2 \leq \left\| \begin{pmatrix} A_k & -B_k^T \\ B_k & C_k \end{pmatrix} \right\|_2 = \|\log_m(V_k)\|_2$. Because C_{k+1} is but the lower diagonal subblock of $\log_m(V_k W)$, the higher-order terms are bounded by $\|\text{h.o.t.}(5)\|_2 \leq \sum_{l=5}^{\infty} \|\log_m(V_k)\|_2^{l-1} \|\Gamma\|_2 \leq \frac{6}{6-\delta^2} \|C_k\|_2 \frac{\delta^4}{1-\delta}$, see [40, Lemma A.1]. The claim is now a straightforward consequence. \square

Proposition 7 shows that with smaller values of δ , the Sylvester approach becomes more and more favorable. The actual value of δ depends on how close the inputs U, \tilde{U} are. For $\delta \approx 0.7147$ the bounds for the asymptotic convergence rates are the same for

both the approaches “Flag_Sylv on/off”; for $\delta \approx 0.3286$ the rate of the Sylvester-based method is improved a factor of 2 and by a factor of 10 for $\delta \approx 0.1270$. Note that in both cases, the bounds overestimate the true convergence rates.

The main computational effort of [Algorithm 4](#) is in the computation of the matrix logarithm in step 5. This can be achieved efficiently (and without resorting to complex numbers arithmetics) by first computing a real Schur form. Assuming that the principal matrix logarithm is properly defined, the Schur form of an orthogonal matrix is block-diagonal with blocks (1) of size (1×1) and (2×2) -blocks of the form $\begin{pmatrix} \cos(\varphi) & -\sin(\varphi) \\ \sin(\varphi) & \cos(\varphi) \end{pmatrix}$, the matrix logarithm of such a block being $\begin{pmatrix} 0 & -\varphi \\ \varphi & 0 \end{pmatrix}$. This is exploited in the actual implementation.

3.5. A geodesic Newton method for the Stiefel logarithm. The nonlinear matrix equation (14) can be cast in the following form

$$V^T F \begin{pmatrix} A & -B^T \\ B & C \end{pmatrix} = I, \quad \text{where } V = \begin{pmatrix} M & X_0 \\ N & Y_0 \end{pmatrix} \in SO(2p).$$

For brevity, introduce

$$\widehat{F} : \text{skew}(2p) \rightarrow SO(2p), \quad S \mapsto V^T F(S).$$

The parameter domain $\text{skew}(2p)$ has a vector space structure that allows to employ Euclidean techniques. The co-domain, however is the Lie group $SO(2p)$. Ignoring the structure of $SO(2p)$, the classical Newton method can be applied to the root finding problem $V^T F(S) - I = 0$. Given a starting point S_0 , the Newton method requires to solve the Taylor-linearized problem

$$I = \widehat{F}(S) + D\widehat{F}_S(H) \approx \widehat{F}(S + H)$$

so that the update H is determined by the linear system $D\widehat{F}_S(H) = I - \widehat{F}(S)$. Yet, the left-hand side and the right-hand side are not compatible, as $\widehat{F}(S) \in SO(2p)$ and $D\widehat{F}_S(H) \in T_{\widehat{F}(S)}SO(2p) = \widehat{F}(S) \text{skew}(2p)$.

A remedy is to replace the Euclidean first-order Taylor approximation, which can be thought of as progressing along a straight line, by moving along a geodesic in the same direction. This leads to a first-order approximation that preserves the Riemannian structure

$$\widehat{F}(S + H) \approx \text{Exp}_{\widehat{F}(S)}(D\widehat{F}_S(H)).$$

On $SO(2p)$, the geodesic that starts from $\widehat{F}(S)$ in the direction of $D\widehat{F}_S(H)$ is

$$\text{Exp}_{\widehat{F}(S)}(D\widehat{F}_S(H)) = \widehat{F}(S) \exp_m(\widehat{F}(S)^T D\widehat{F}_S(H)),$$

see, e.g., [13]. The first-order approximation to (14) becomes

$$(20) \quad I = \widehat{F}(S) \exp_m(\widehat{F}(S)^T D\widehat{F}_S(H)) \quad \Leftrightarrow \quad \underbrace{\widehat{F}(S)^T D\widehat{F}_S(H)}_{\text{skew}} = \underbrace{\log_m(\widehat{F}(S)^T)}_{\text{skew}}.$$

The left-hand side is a linear operator

$$L_S : \text{skew}(2p) \rightarrow \text{skew}(2p), \quad H \mapsto \widehat{F}(S)^T D\widehat{F}_S(H).$$

In summary, this leads to the iterative scheme stated in [Algorithm 5](#). Upon convergence, $S_k = \begin{pmatrix} A_k & -B_k^T \\ B_k & C_k \end{pmatrix}$ is found and the output $\Delta := \text{Log}_U^{St}(\tilde{U}) = UA_k + QB_k \in T_U$ is formed with U, Q as in [Algorithm 4](#). Computationally, the expensive part is to evaluate the operator L_S . For convenience, let us restrict to the Euclidean metric and write

$$S = \begin{pmatrix} A & -B^T \\ B & C \end{pmatrix}, \quad S_{\text{tri}} = \begin{pmatrix} 2A & -B^T \\ B & 0 \end{pmatrix}, \quad S_{\text{di}} = \begin{pmatrix} A & 0 \\ 0 & C \end{pmatrix},$$

likewise for $H \in \text{skew}(2p)$. It holds

$$(21) \quad \begin{aligned} L_S(H) &= \widehat{F}(S)^T D\widehat{F}_S(H) = F(S)^T VV^T DF_S(H) \\ &= F(S)^T (D(\exp_m)_{S_{\text{tri}}}(H_{\text{tri}}) \exp_m(-S_{\text{di}}) + \exp_m(S_{\text{tri}}) D(\exp_m)_{S_{\text{di}}}(-H_{\text{di}})). \end{aligned}$$

In an implementation, we do not actually form this operator, but implement its action on a matrix H . This is then used in a matrix-free version of the GMRES algorithm [31] (as pre-installed in Matlab, version R2019b). For the practical evaluation of $D(\exp_m)_S(H)$, we use Mathias' Theorem [15, Thm 3.6], which simultaneously gives $\exp_m(S)$. An equivalent alternative to (14) is to solve

Algorithm 5 GeoNewton for solving (14)

- 1: $k = 0$
 - 2: **while** $\|\log_m(\widehat{F}(S_k)^T)\|_F > \tau$ **do**
 - 3: solve $L_{S_k}(H_k) = \log_m(\widehat{F}(S_k)^T)$
 - 4: update $S_{k+1} = S_k + H_k$
 - 5: $k = k + 1$
 - 6: **end while**
-

$$(22) \quad 0 = \log_m(F(S)) - \log_m(V).$$

In this form, both the unknown S and the output $\log_m(F(S)) - \log_m(V)$ are in the vector space $\text{skew}(2p)$ so that this equation is amenable to be treated with the classical Newton method. However, computing or approximating the derivative remains the computational bottleneck. The associated linear operator now involves differentials of both the matrix exponential and the matrix logarithm. We tackle this with the same strategy as above by relying on Mathias' Theorem and the matrix-free GMRES method. The matrix functions $\exp_m(S)$ and $\log_m(S)$ may be approximated via the Cayley transformation $\text{Cay}(S) = (I - \frac{1}{2}S)^{-1}(I + \frac{1}{2}S)$ and its inverse; likewise the differentials of $D(\exp_m)_S(H)$ and $D(\log_m)_S(H)$ may be approximated with the differentials of the corresponding Cayley transformations.

We mention these approaches for the sake of completeness and include the algorithms based on (20) and (22) in the algorithmic competition. However, the numerical experiments show that none of the above approaches can't compete, neither with the p -shooting method [Algorithm 2](#) nor with the algebraic Stiefel log algorithm [Algorithm 4](#). This also holds, when the Cayley transformations are used to replace \exp_m and \log_m . Therefore, we omit a detailed discussion.

4. Numerical experiments. In this section, we conduct various numerical experiments for assessing the performance of the proposed approaches to solve the local

geodesic endpoint problem. All experiments are performed with Matlab R2019b on a Linux 64bit HP notebook with four Intel(R) Core(TM) i7-5600U 2.60GHz CPUs.⁴

(Sec. 4.1) Test Case 1: random data $n = 2000$, $p = 500$, canonical metric, 5 runs			
$\text{dist}(U, \tilde{U}) = 5\pi$			
Method	av. rel. error $\ \Delta - \Delta_{rec}\ _\infty$	av. iter. count	av. time
Alg. 4	$0.50 \cdot 10^{-11}$	13.0	13.00s
Alg. 4+Sylv.	$0.29 \cdot 10^{-12}$	7.0	8.29s
Alg. 4+Sylv.+Cay.	$0.29 \cdot 10^{-12}$	7.0	8.27s
Alg. 2 on 2 steps	$0.49 \cdot 10^{-11}$	41.0	25.53s
Alg. 2 on 4 steps	$0.61 \cdot 10^{-11}$	35.0	53.89s
Alg. 1 on 2 steps	$0.51 \cdot 10^{-11}$	39.8	34.06s
Single shooting [35, §2.3]	unfeasible du to memory overflow		
(Sec. 4.1) Test Case 2: random data $n = 120$, $p = 30$, canonical metric, 10 runs			
$\text{dist}(U, \tilde{U}) = \pi$			
Method	av. rel. error $\ \Delta - \Delta_{rec}\ _\infty$	av. iter. count	av. time
Alg. 4	$0.226 \cdot 10^{-11}$	10.2	0.027s
Alg. 4+Sylv.	$0.159 \cdot 10^{-11}$	5.0	0.018s
Alg. 4+Sylv.+Cay.	$0.160 \cdot 10^{-11}$	5.0	0.018s
Alg. 2 on 2 steps	$0.291 \cdot 10^{-11}$	26.8	0.033s
Alg. 2 on 4 steps	$0.193 \cdot 10^{-11}$	24.7	0.064s
Alg. 1 on 2 steps	$0.281 \cdot 10^{-11}$	26.4	0.032s
Single shooting [35, §2.3]	$0.58 \cdot 10^{-14}$ (results for 1 run.)	5	524.6s
(Sec. 4.1) Test Case 3: random data $n = 12$, $p = 3$, canonical metric, 100 runs			
$\text{dist}(U, \tilde{U}) = 0.95\pi$ (averaging only over the converged runs)			
Method	av. rel. error $\ \Delta - \Delta_{rec}\ _\infty$	av. iter. count	av. time
Alg. 4	$0.62 \cdot 10^{-10}$ (1 run not conv'd)	120.3	0.046s
Alg. 4+Sylv.	$0.50 \cdot 10^{-10}$ (1 run not conv'd)	41.1	0.023s
Alg. 4+Sylv.+Cay.	$0.53 \cdot 10^{-10}$ (1 run not conv'd)	41.3	0.021s
Alg. 2 on 2 steps	(all 100 runs not conv'd)	–	–
Alg. 2 on 4 steps	$0.80 \cdot 10^{-10}$ (all 100 runs conv'd.)	212.2	0.031s
Alg. 1 on 2 steps	(all 100 runs not conv'd)	–	–
Single shooting [35, §2.3]	$0.42 \cdot 10^{-14}$ (41 runs not conv'd.)	7.93	0.021s

TABLE 1

Numerical performance for the cases considered in Subsection 4.1.

4.1. The geodesic endpoint problem for the canonical metric. We create two points U, \tilde{U} pseudo-randomly on $St(n, p)$, but such that they are a prescribed geodesic distance apart. More precisely, we construct U from a QR-decomposition of a random $(n \times p)$ -matrix with entries sampled from the uniform distribution. Then, we create a random tangent vector $\Delta = UA + (I - UU^T)T$, where $A \in \mathbb{R}^{p \times p}$ is random but skew and $T \in \mathbb{R}^{n \times p}$ is random. Then, Δ is scaled to the prescribed length according to the Riemannian metric and $\tilde{U} \in St(n, p)$ is obtained as $\tilde{U} = \text{Exp}_U(\Delta)$.

Then, the various Stiefel-log algorithms are applied to compute the reconstructed tangent vector Δ_{rec} and the absolute accuracy is checked in the infinity-matrix norm.

⁴The Matlab code and an accompanying Python implementation is available on https://github.com/RalfZimmermannSDU/RiemannStiefelLog/tree/main/Stiefel_log_general_metric/

In summary, we perform the following three steps

$$(a) \quad \tilde{U} \leftarrow \text{Exp}_U(\Delta), \quad (b) \quad \Delta_{\text{rec}} \leftarrow \text{Log}_U(\tilde{U}), \quad (c) \quad \text{compute } \|\Delta - \Delta_{\text{rec}}\|_{\infty}.$$

We perform 10 runs with random data, record the numerical accuracy, the iteration count and the computation time and average over the results. In order to evaluate the logarithm, we use the following methods:

- Alg. 4 as in [40].
- Alg. 4 enhanced by the Sylvester equation (19) as detailed in Subsection 3.4.
- Alg. 4 enhanced by (19) and with the Cayley transformation replacing the matrix exponential in Step 15.
- Alg. 2 on two time steps $\{0.0, 1.0\}$ in the unit interval $[0, 1]$.
- Alg. 2 on four time steps $\{0.0, 0.3, 0.6, 1.0\}$ of the unit interval $[0, 1]$.
- Alg. 1 on two time steps $\{0.0, 1.0\}$ in the unit interval $[0, 1]$.
- The single shooting method of [35, Section 2.3] that is based on a Newton root finding problem under the canonical metric.

In each case, the convergence threshold is set to $\tau = 10^{-11}$. Table 1 displays the results for data on $St(n = 2000, p = 500)$ with $\text{dist}(U, \tilde{U}) = 5\pi$, for data on $St(n = 120, p = 30)$ with $\text{dist}(U, \tilde{U}) = \pi$ and for data on $St(n = 12, p = 3)$ with $\text{dist}(U, \tilde{U}) = 0.95\pi$. Example plots of the convergence histories are shown in Figure 8 and Figure 9 of the supplements, respectively.

The table shows that Algorithm 4 with “Flag_Sylv on” exhibits the best performance for the cases considered in regards of the computation time. In terms of the numerical accuracy it is outranked by the Newton-based single shooting method of [35, Section 2.3], provided that the latter converges. It can also be seen that a subdivision of the interval $[0, 1]$ is not required for Algorithm 2 in order to converge for the larger data sets under consideration. The dimensions and distance for the low-dimensional data set on $St(12, 3)$ are chosen as in [36], where the global geodesic endpoint problem is considered. Recall that the estimated injectivity radius of $St(n, p)$ under the canonical metric is at least 0.89π and most likely not larger, see [29]. In fact, the methods considered here are local by nature. As is to be expected, in the experiments, we observe convergence in some cases and divergence in other cases, see Table 1 for details. The Algorithm 2 on four time steps in $[0, 1]$ converges in all cases considered, while it diverges in all cases, if only the boundary points of $[0, 1]$ are considered in the discrete parallel transport.

4.2. The geodesic endpoint problem for the Euclidean metric. In this section, we repeat the experiments of Subsection 4.1 with exactly the same set-up, but for the Euclidean metric. Since the algebraic Stiefel log algorithm Algorithm 4 is not available for metrics other than the canonical one, we juxtapose the following methods

- Alg. 5, “GeoNewton”, the geodesic Newton method for (14).
- Alg. “EucNewton”, based on the classical Newton method for solving (22).
- Alg. 2 on two time steps $\{0.0, 1.0\}$ of the unit interval $[0, 1]$.
- Alg. 2 on four time steps $\{0.0, 0.3, 0.6, 1.0\}$ of the unit interval $[0, 1]$.

In each case, the convergence threshold is set to $\tau = 10^{-11}$. Table 2 displays the results for data on $St(n = 120, p = 30)$ with $\text{dist}(U, \tilde{U}) = \pi$ and for data on $St(n = 2000, p = 500)$ with $\text{dist}(U, \tilde{U}) = 5\pi$. In the latter case, only one random run is performed due to the large computation times for the Newton methods. Example plots of the convergence histories are shown in Figure 11 and Figure 12 of the supplements, respectively.

The table shows that [Algorithm 2](#) without a subdivision of $[0, 1]$ exhibits the best performance in terms of the computation time for the cases considered here. For the test case with data on $St(2000, 500)$, the method is ca. 90 times faster than the Newton-based methods and also much more memory efficient, since no large linear operators need to be constructed. These computation times are representative for other values of α in the family of Riemannian metrics.

4.3. Investigations on the parametric dependencies. In this section, the performance of the proposed methods for computing $\text{Log}_U^\alpha(\tilde{U})$ with $U, \tilde{U} \in St(n, p)$ is investigated under changes in the metric parameter α , the Riemannian distance of the input points $\text{dist}(U, \tilde{U})$ as well as the matrix dimensions n and p .

We start with assessing the performance of [Algorithm 2](#) for metric parameters $\alpha \in (-1, \infty)$, where the associated metric is Riemannian. (For $\alpha \in (-\infty, -1)$, the metric becomes pseudo-Riemannian, see [[17](#), Section 5.5].) To this end, we fix the dimensions $n = 200$, $p = 50$ and construct pseudo-random data $U \in St(200, 50)$, $\Delta_0 \in T_U St(200, 50)$ as described in [Subsection 4.1](#). We discretize the parameter interval $[-0.9, 5.0]$ with equidistant steps of size 0.05. For each value $\alpha \in \{-0.9 + 0.05j | j = 0, \dots, 118\}$, we compute $\Delta(\alpha) = \frac{d}{\|\Delta_0\|_\alpha} \Delta_0$, so that $\Delta(\alpha)$ is normalized to a length of d according to the α -metric. As a distance factor, we use $d = 0.5\pi$. Then, we set $\tilde{U} = \text{Exp}_U^\alpha(\Delta(\alpha))$ with the Stiefel exponential computed according to [\(11\)](#). In this way, a Stiefel data pair U, \tilde{U} with $\text{dist}_\alpha(U, \tilde{U}) = d = 0.5\pi$ is obtained. We apply [Algorithm 2](#) to compute $\text{Log}_U^\alpha(\tilde{U})$ up to a convergence threshold of $\tau = 10^{-11}$ and record the wall clock computation time as well as the iteration count. The results are displayed in [Figure 2](#). The supplements feature an analog experiment with data on $St(2000, 200)$, see [Figure 13](#).

In both test cases, the iteration count is minimal precisely at $\alpha = -\frac{1}{2}$, which corresponds to the Euclidean metric. We conjecture that the dependency of the iteration count on the metric parameter α is curvature-related. Recall that the curvature of a Riemannian manifold depends on the metric. Furthermore, observe that in the flat matrix space $\mathbb{R}^{n \times p}$, the shooting method produces the correct solution after one single iteration, because the geodesics are straight lines so that $\text{Exp}_U(t\Delta) = U + t\Delta$.

(Sec. 4.2) Test Case 1: random data $n = 2000$, $p = 500$, Euclidean metric, 1 run				
$\text{dist}(U, \tilde{U}) = 5\pi$				
Method	rel. error $\ \Delta - \Delta_{rec}\ _\infty$	iter. count	time	
Alg. 5 GeoNewton	$0.61 \cdot 10^{-11}$	13	958.2s	
Alg. EucNewton	$0.23 \cdot 10^{-11}$	6	890.1s	
Alg. 2 on 2 steps	$0.26 \cdot 10^{-11}$	20	10.5s	
Alg. 2 on 4 steps	$0.36 \cdot 10^{-11}$	11	14.8s	

(Sec. 4.2) Test Case 2: random data $n = 120$, $p = 30$, Euclidean metric, 10 runs				
$\text{dist}(U, \tilde{U}) = \pi$				
Method	av. rel. error $\ \Delta - \Delta_{rec}\ _\infty$	av. iter. count	av. time	
Alg. 5 GeoNewton	$0.11 \cdot 10^{-11}$	8.0	0.34s	
Alg. EucNewton	$0.071 \cdot 10^{-11}$	5.0	0.85s	
Alg. 2 on 2 steps	$0.078 \cdot 10^{-11}$	13.1	0.016s	
Alg. 2 on 4 steps	$0.12 \cdot 10^{-11}$	9.0	0.030s	

TABLE 2
Numerical performance for the cases considered in [Subsection 4.2](#).

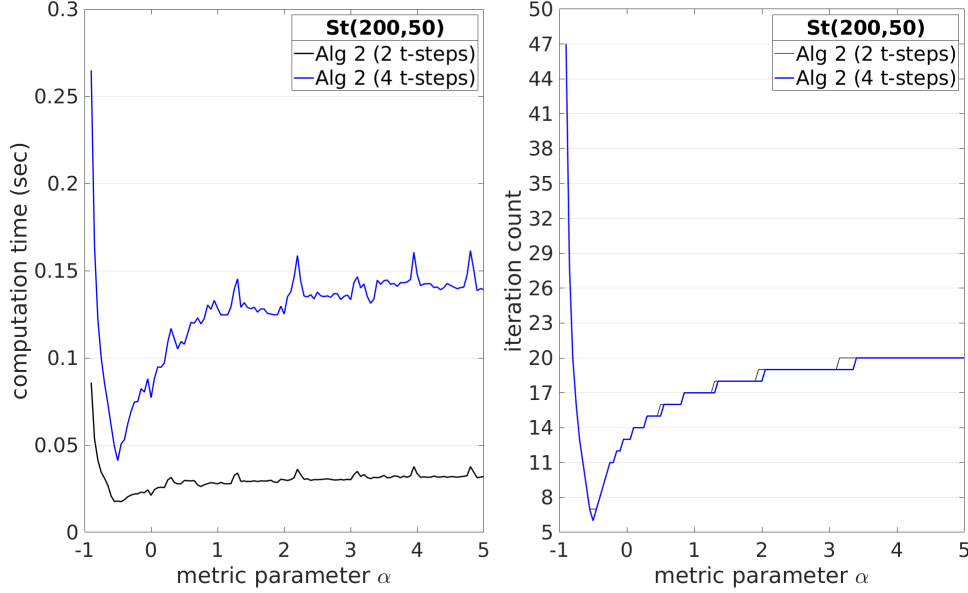


FIG. 2. (cf. Subsection 4.3) Wall clock computation time in seconds versus α (left) and iteration count until convergence versus α (right) for computing $\text{Log}_U^\alpha(\tilde{U})$ with Algorithm 2. The trial parameter set is $\{\alpha = -0.9 + 0.05j \mid j = 0, \dots, 118\}$. The data points $U, \tilde{U} \in \text{St}(200, 50)$ are at a Riemannian α -distance of $\text{dist}_\alpha(U, \tilde{U}) = 0.5\pi$. Timing results are averaged over 100 runs.

Following this line of reasoning, the experimental results suggest that at least locally around the generic pseudo-random data points, $(\text{St}(n, p), \langle \cdot, \cdot \rangle^\alpha)$ is least curved for the induced Euclidean metric, where $\alpha = -\frac{1}{2}$.

Next, we assess the dependency of Algorithm 2 and Algorithm 4 on the distance of the input parameters U, \tilde{U} under the canonical metric. As in Subsection 4.1, we construct $U \in \text{St}(n, p)$ and $\Delta_0 \in T_U \text{St}(n, p)$. Then, we scale $\Delta(d) = \frac{d}{\|\Delta_0\|_0} \Delta_0$ and set $\tilde{U} = \text{Exp}_U^0(\Delta(d))$ so that by construction, $\text{dist}(U, \tilde{U}) = d$ with respect to the canonical metric ($\alpha = 0$). We consider distance factors of $d = 0.5\pi, 1.0\pi, \dots, 4.5\pi$ and measure the wall clock time and the iteration count until the numerical convergence measure drops below a threshold parameter of $\tau = 10^{-11}$. The results are displayed in Figure 3. It can be seen that for Algorithm 4, the iteration count and wallclock time grow moderately with increasing distance. In contrast, time and iteration count associated with Algorithm 2 on two time steps exhibit a strong nonlinear dependency on the distance. For Algorithm 2 on four time steps, the growth in time and number of iterations is roughly linear but with a steeper slope when compared to Algorithm 4.

Lastly, we expose the dependency of Algorithm 1, Algorithm 2 and Algorithm 4 on the dimensions n and p . Again, we resort to the canonical metric ($\alpha = 0$). We fix p to a value of $p = 200$ and vary $n = 1000 \cdot 2^j$ with $j = 1, \dots, 8$. Pseudo-random data $U, \tilde{U} \in \text{St}(n, p)$ with $\text{dist}_0(U, \tilde{U}) = 1.5\pi$ is constructed as in Subsection 4.1. We run the various algorithms with a target accuracy of $\tau = 10^{-10}$ and measure the wall clock computation time as well as the iteration count. Figure 4 displays the results.

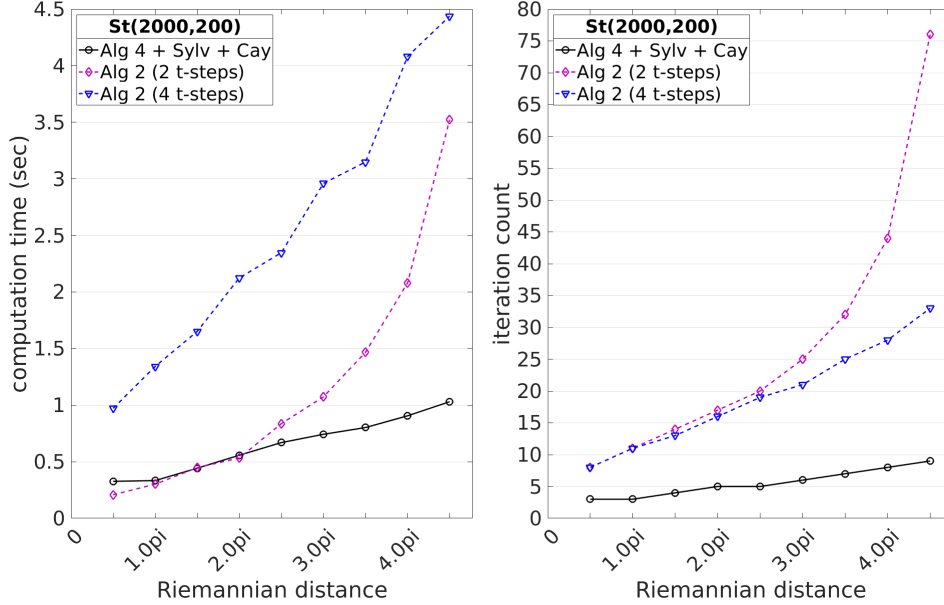


FIG. 3. (cf. [Subsection 4.3](#)) Left: Wall clock computation time in seconds versus $d = \text{dist}(U, \tilde{U})$. Right: Iteration count versus $d = \text{dist}(U, \tilde{U})$. The trial parameter set is $\{d = (0.5 + 0.5j) \cdot \pi \mid j = 0, \dots, 8\}$. The data points are $U, \tilde{U} \in \text{St}(2000, 200)$. Timing results are averaged over 20 runs.

The associated measurement data for $j = 3, \dots, 8$ is listed in [Table 3](#). It can be observed that [Algorithm 2](#) and the variants of [Algorithm 4](#) perform comparably, while [Algorithm 1](#) is roughly one order of magnitude slower. This is expected, because the former methods address a matrix problem that scales in the dimension p in the associated loop iterations, but they share matrix multiplications and a QR-decomposition of n -by- p matrices as pre- and postprocessing steps.

Method	$n = 8k$	$n = 16k$	$n = 32k$	$n = 64k$	$n = 128k$	$n = 256k$
Alg. 4	0.719s	0.873s	1.25s	2.02s	3.67s	6.87s
Alg. 4+Sylv.	0.620s	0.739s	1.03s	1.80s	3.36s	6.59s
Alg. 4+Sylv.+Cay.	0.582s	0.756s	1.11s	1.81s	3.29s	6.64s
Alg. 2 (2 t-steps)	0.522s	0.623s	0.930s	1.74s	3.27s	6.46s
Alg. 1 (2 t-steps)	3.28s	5.22s	10.63s	21.5s	39.2s	unfeasible

TABLE 3

(cf. [Subsection 4.3](#)) Wallclock computation time for the results displayed in [Figure 4](#).

We repeat the experiment with fixed $n = 6000$ and $p = 10 \cdot 2^j$ with $j = 1, \dots, 8$. [Figure 5](#) displays the results. The associated measurement data for $j = 3, \dots, 8$ is listed in [Table 4](#). It can be observed that for the dimensions tested, [Algorithm 2](#) is fastest until a column-dimension of $p = 320$. Beyond this point, [Algorithm 4](#) with the Sylvester enhancement takes the lead. For $p = 2560$, the wallclock run time of [Algorithm 4](#) is a factor of 0.82 smaller than the runtime of [Algorithm 2](#).

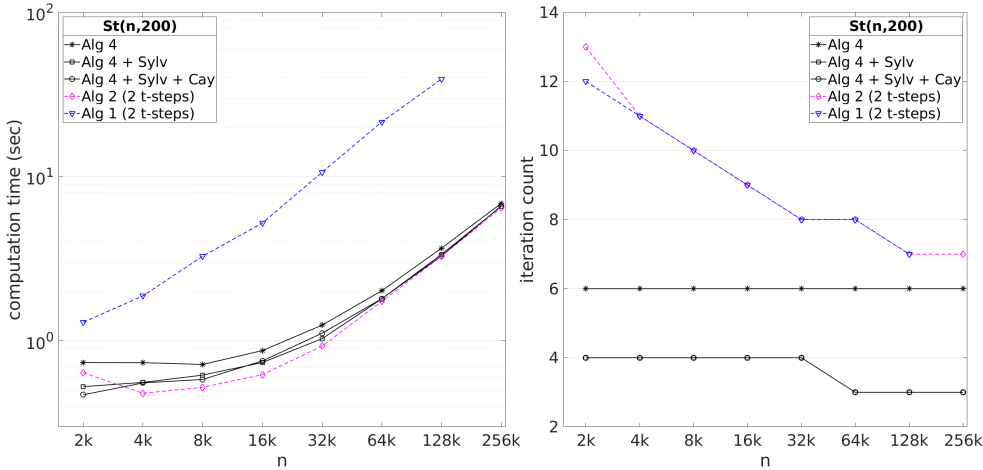


FIG. 4. (cf. Subsection 4.3) Left: Wall clock computation time in seconds versus matrix dimension n on a log-log scale. Right: Iteration count versus matrix dimension n on a log-linear scale. The trial parameter set is $\{n = 1000 \cdot 2^j \mid j = 1, \dots, 8\}$. The data points $U, \tilde{U} \in St(n, 200)$ are at a canonical Riemannian distance of $\text{dist}_\alpha(U, \tilde{U}) = 1.5\pi$. (The case of $St(256k, 200)$ was not treatable with Algorithm 1 on the given laptop computer.)

Method	$p = 80$	$p = 160$	$p = 320$	$p = 640$	$p = 1280$	$p = 2560$
Alg. 4	0.134s	0.474s	2.12s	11.44s	87.31s	423.3s
Alg. 4+Sylv.	0.088s	0.343s	1.27s	7.68s	53.81s	363.0s
Alg. 4+Sylv.+Cay.	0.086s	0.342s	1.28s	7.55s	52.80s	355.1s
Alg. 2 (2 t-steps)	0.076s	0.226s	1.20s	9.87s	61.78s	432.3s
Alg. 1 (2 t-steps)	0.477s	1.336s	4.82s	23.28s	112.6s	564.0s

TABLE 4

(cf. Subsection 4.3) Wallclock computation time for the results displayed in Figure 5.

4.4. The impact of the metric on interpolating matrix factorizations.

In this subsection, we consider the practical problems of interpolating the QR-decomposition and the SVD of time-dependent matrix curves. Let $n > m > p$. For a compact QR-decomposition $Y = QR$ of a rectangular matrix $Y \in \mathbb{R}^{n \times p}$, it holds $Q \in St(n, p)$. If the SVD is used to produce the best rank- p approximation of a given matrix $\mathbb{R}^{n \times m} \ni Y \approx U_p \Sigma_p V_p^T$, then $U_p \in St(n, p), V_p \in St(m, p)$. Hence, in both applications, interpolation of matrix sample data on the Stiefel manifold has to be considered. We will investigate how the choice of the metric affects the resulting interpolant.

The standard approach to interpolating manifold-valued data is (1) to select a base point, (2) to apply the Riemannian logarithm to map the data set to the tangent space at the chosen base point, (3) to perform interpolation in the tangent space, (4) to map the results back to the manifold via the Riemannian exponential.

First, we reproduce the example from [41, Section 5.2] and consider a cubic matrix polynomial

$$t \mapsto Y(t) = Y_0 + tY_1 + t^2Y_2 + t^3Y_3, \quad Y_k \in \mathbb{R}^{n \times p}, \quad n = 500, p = 10.$$

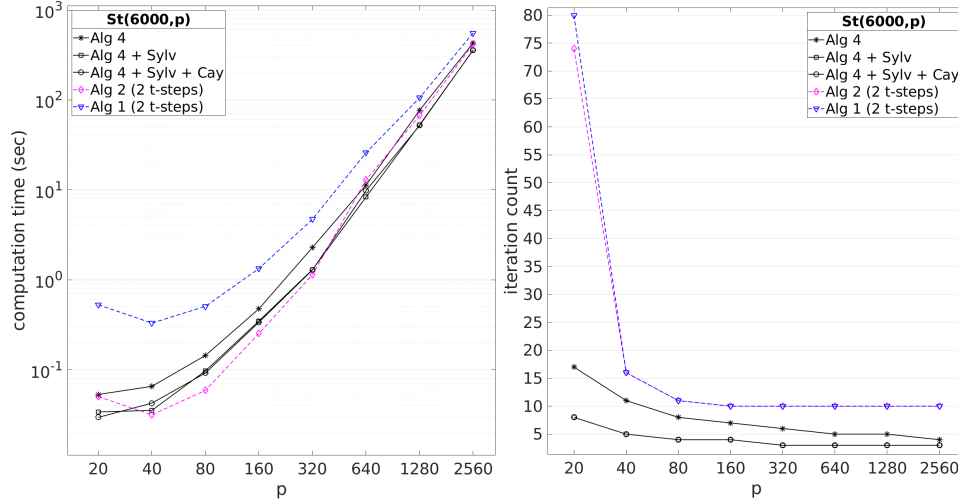


FIG. 5. (cf. [Subsection 4.3](#)) Left: Wall clock computation time in seconds versus matrix dimension p on a log-log scale. Right: Iteration count versus matrix dimension p on a log-linear scale. The trial parameter set is $\{p = 10 \cdot 2^j \mid j = 1, \dots, 8\}$. The data points $U, \tilde{U} \in St(6000, p)$ are at a canonical Riemannian distance of $\text{dist}_\alpha(U, \tilde{U}) = 1.5\pi$.

The matrices Y_k are produced as random matrices with entries uniformly sampled from $[0, 1]$ for Y_0 , entries uniformly sampled from $[0, 0.5]$ for Y_1, Y_2 and from $[0, 0.2]$ for Y_3 . Then, $Y(t)$ is sampled at 5 equidistant samples $t_i \in \{-1.1, -0.55, 0.0, 0.55, 1.1\}$. At each sample point t_i , the Q-factor $Q(t_i) \in St(n, p)$ of the QR-decomposition is computed. We employ radial basis function (RBF) interpolation in the tangent space with the cubic RBF and three-point cubic spline interpolation, for details, see [\[41\]](#). For mapping the sample data back and forth between the Stiefel manifold and its tangent space as sketched in [Figure 1](#), we use the Riemannian exponential and logarithm under the α -metric. We start at $\alpha = -0.8$ and proceed until $\alpha = 2.04$ in steps of $\delta\alpha = 0.02$.

For each value of α , the relative interpolation errors are computed at 101 equidistant instants $t_j = -1.1 + j\delta t \in [-1.1, 1.1]$, $\delta t = 0.022$, $j = 0, 1, \dots, 100$ in the matrix Frobenius norm

$$e_\alpha(t_j) := \frac{\|Q_\alpha^*(t_j) - Q(t_j)\|_F}{\|Q(t_j)\|_F}.$$

Here, $Q_\alpha^*(t_j)$ denotes the manifold interpolant under the α -metric and $Q(t_j)$ is the reference solution. The associated discrete L_2 -norm of the error is computed as $\text{err}_{L_2}(\alpha) = \sqrt{\delta t \sum_{j=0}^{100} e_\alpha(t_j)^2}$. The error graphs $\alpha \mapsto \text{err}_{L_2}(\alpha)$ for both interpolation methods under consideration are displayed in [Figure 6](#). The discrete arrays that underlie the graphs feature both a global minimum at a similar location. For RBF interpolation, the total L_2 error is lowest at $\alpha = 0.28$. For three-point cubic spline interpolation, the global minimum is at $\alpha = 0.26$. It can also be seen that beyond $\alpha \geq -0.1$, the impact of the metric on the error is rather negligible. It should also be emphasized, that the largest and the smallest tested errors differ only by a small absolute amount.

As a second test case, we rework the example from [\[41, Section 5.3\]](#) and con-

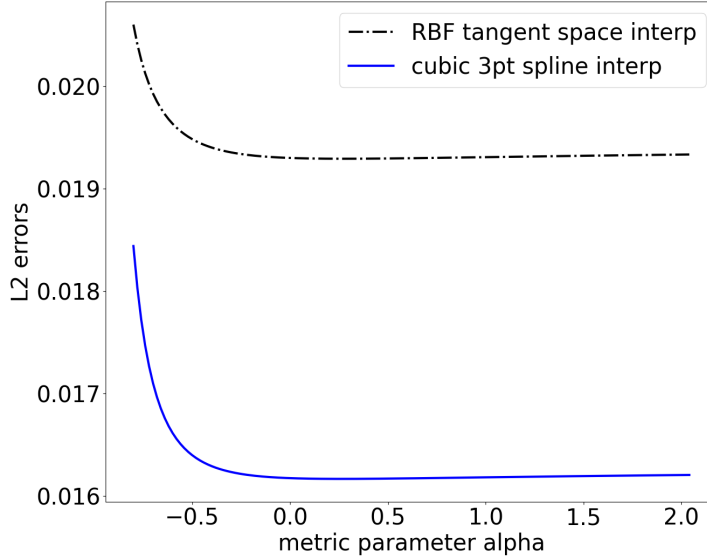


FIG. 6. (cf. [Subsection 4.4](#)) Total L_2 errors versus α associated with interpolating the Q -factor of a time-dependent curve of QR-factorizations under varying the α -metric. The tested α -range is $[-0.8, 2.04]$ on steps of size $\delta\alpha = 0.02$.

struct a nonlinear matrix function with fixed low rank. We start with a cubic matrix polynomial

$$Y(t) = Y_0 + tY_1 + t^2Y_2 + t^3Y_3, \quad Y_i \in \mathbb{R}^{n \times r}, n = 10\,000, r = 10$$

with random matrices Y_k with entries uniformly sampled from $[0, 1]$ for Y_0 and from $[0, 0.5]$ for Y_1, Y_2, Y_3 . Then, a second matrix polynomial is considered

$$Z(t) = Z_0 + tZ_1 + t^2Z_2, \quad Z_i \in \mathbb{R}^{r \times m}, r = 10, m = 300.$$

Here, the entries of Z_0 are sampled uniformly from $[0, 1]$ while the entries of Z_1, Z_2 are sampled uniformly from $[0, 0.5]$. The nonlinear low-rank matrix function is set to be

$$W(t) = Y(t)Z(t) \in \mathbb{R}^{n \times m}.$$

We will conduct cubic Hermite interpolation. To this end, the low-rank SVD

$$W(t) = U_r(t)\Sigma_r(t)V_r(t)^T, \quad U_r(t) \in St(n, r), \quad V_r(t) \in St(m, r), \quad \Sigma \in \mathbb{R}^{r \times r}$$

and the associated matrix derivatives are sampled at three Chebychev nodes $t_0 \approx 0.0603, t_1 = 0.45, t_2 = 0.8397$ in the interval $[0.0, 0.9]$. The Hermite sample data set is

$$U_r(t_i), \dot{U}_r(t_i), \quad V_r(t_i), \dot{V}_r(t_i), \quad \Sigma_r(t_i), \dot{\Sigma}_r(t_i), \quad i = 0, 1, 2,$$

see [\[41, Section 5.3\]](#) for details.

We conduct Hermite interpolation under the α -metric, starting from $\alpha = -0.75$ and proceeding up to $\alpha = 1.5$ in steps of $\delta\alpha = 0.05$. (For $\alpha < -0.75$ and $\alpha > 1.5$,

convergence issues occurred when mapping the sample data set to the tangent space with the Riemannian logarithm.)

For each value of α , the relative interpolation errors are computed at 100 equidistant instants $t_j \in [t_0, t_2]$ in the matrix Frobenius norm as

$$e_\alpha(t_j) = \frac{\|U^*(t_j)\Sigma^*(t_j)(V^*(t_j))^T - W(t_j)\|_F}{\|W(t_j)\|_F},$$

where $U^*(t_j)$, $\Sigma^*(t_j)$, $V^*(t_j)$ are the interpolants of the matrix factors of the low-rank SVD of $W(t_j)$ and $W(t_j)$ is the reference solution. The associated discrete L_2 -norm of

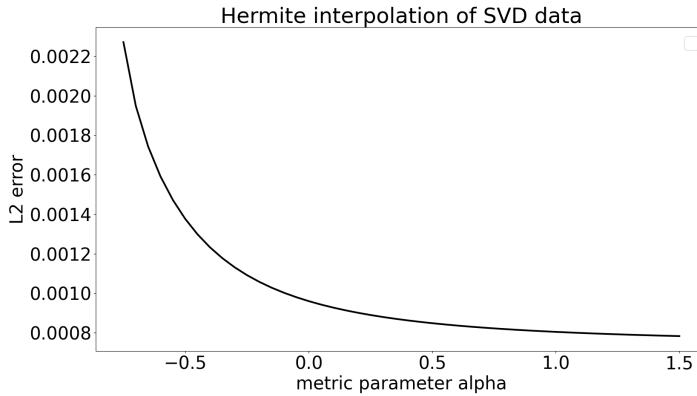


FIG. 7. (cf. [Subsection 4.4](#)) Total L_2 errors versus α associated with Hermite-interpolating a time-dependent curve of low-rank SVDs under varying the α -metric. The tested α -range is $[-0.75, 1.5]$ on steps of size $\delta\alpha = 0.05$.

the error is computed as $\text{err}_{L_2}(\alpha) = \sqrt{\delta t \sum_{j=0}^{99} e_\alpha(t_j)^2}$. The error graph $\alpha \mapsto \text{err}_{L_2}(\alpha)$ is displayed in [Figure 7](#). It can be seen that in the tested α -range, the total L_2 error is largest at the left bound $\alpha = -0.75$ and decreases monotonically with increasing α . The slope flattens considerably for larger values of α .

5. Discussions. For the canonical metric, the numerical experiments identify the Sylvester-enhanced version of [Algorithm 4](#) as the method of choice: The runtime is comparable to [Algorithm 2](#) on two time steps for the smaller test cases and considerably shorter for the test cases in higher dimensions. Moreover, it is more robust with respect to increasing the distance of the input points, see [Figure 3](#).

For all other α -metrics, the p -shooting method [Algorithm 2](#) on two time steps performs best in terms of the runtime. Yet, data on Stiefel manifolds of smaller dimension or data points that are further apart may necessitate in doing more time steps in the inner loops of [Algorithm 2](#). Even though for all test cases considered in this work, it was sufficient to go up to 4 time steps, [Algorithm 2](#) is a local method and it cannot be expected that increasing the number of inner time steps will make the method converge in all cases. The Euclidean metric ($\alpha = -\frac{1}{2}$) has a special position in the sense that the iteration count of the p -shooting method is lowest for the Stiefel manifold under this choice of metric.

The choice of metric is problem-dependent. We included an experiment on interpolating curves of orthogonal matrix factorizations. When casting this into an interpolation problem on the Stiefel manifold, a metric has to be selected. While

the exact curve is completely independent from the selected metric, the interpolation error is not. Hence, if the computational resources allow for it, a parametric study may be beneficial when selecting the metric for a certain application. Otherwise, the canonical metric presents itself as a natural general purpose tool.

Acknowledgements. The authors would like to thank Marco Sutti for sharing the Matlab code associated with [35]. The second author’s work has been supported in part by the German Federal Ministry of Education and Research (BMBF-Projekt 05M20WWA: Verbundprojekt 05M2020 - DyCA).

Independent from this work and concurrent with our original arXiv submission, the related preprint [25] appeared, which takes a similar starting point to tackle the geodesic endpoint problem but then pursues an optimization approach.

Appendix A. Convergence plots associated with Subsection 4.1. Figures 8, 9 and 10 show the convergence history of a single run associated with Test Case 1, Test Case 2 and Test Case 3 of Table 1, respectively. Note that for Algorithm 4, the convergence measure at iteration k is the norm of the lower diagonal block C_k in (18), while it is the error between the target \tilde{U} and the shooting point \tilde{U}_{shoot} at iteration k for Algorithm 2 and Algorithm 1.

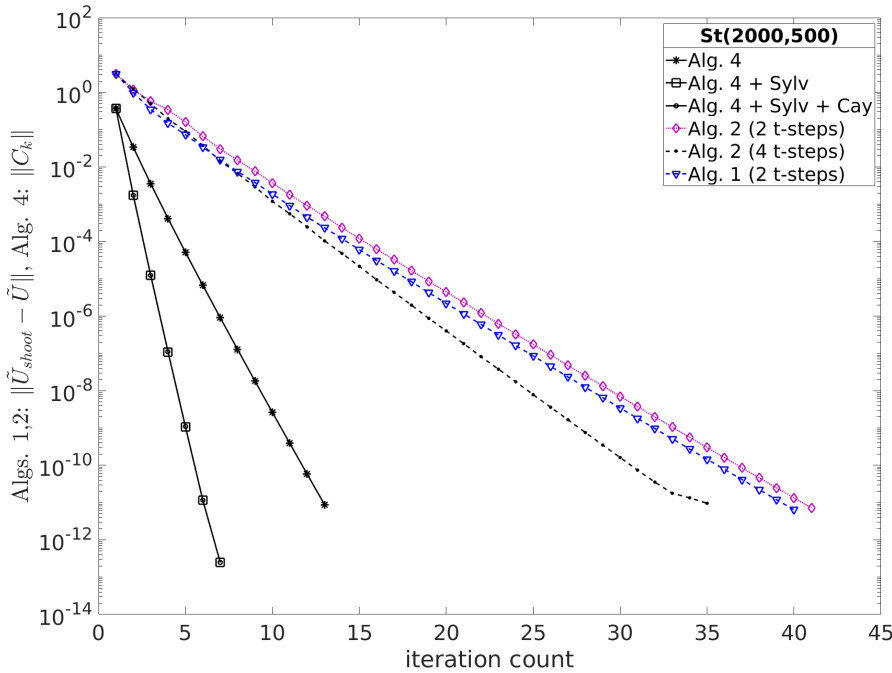


FIG. 8. (cf. Subsection 4.1) Convergence history of the various log-algorithms for computing $\text{Log}_U(\tilde{U})$ for the canonical metric. The graphs show one run of the test case $St(2000, 500)$. The input data is at a Riemannian distance of $\text{dist}(U, \tilde{U}) = 5\pi$.

Appendix B. Convergence plots associated with Subsection 4.2. Figures 11 and 12 show the convergence history of a single run associated with Test Case 1 and Test Case 2 of Table 2, respectively. Note that the convergence measure for Algorithm 2 and Algorithm 1 is the error between the target \tilde{U} and the shooting

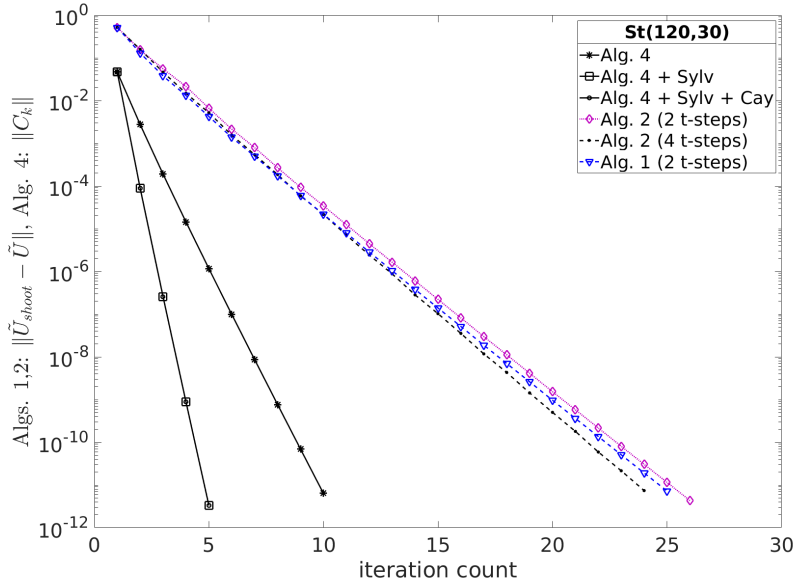


FIG. 9. (cf. [Subsection 4.1](#)) Convergence history of the various log-algorithms for computing $\text{Log}_U(\tilde{U})$ under the canonical metric. The graphs show one run of the test case $St(120,30)$. The input data is at a Riemannian distance of $\text{dist}(U, \tilde{U}) = \pi$.

point \tilde{U}_{shoot} at iteration k , while it is $\|\log_m(\hat{F}(S_k)^T)\|$ for [Algorithm 5](#) and the norm of the right hand side of (22) for Algorithm ‘[EucNewton](#)’.

Appendix C. Additional experiments associated with [Subsection 4.3](#).

We repeat the first experiment of [Subsection 4.3](#) for pseudo-random data $U, \tilde{U} \in St(2000, 200)$. As a distance factor, we use $d = 0.8\pi$. For each value $\alpha \in \{-0.9 + 0.05j | j = 0, \dots, 118\}$, we apply [Algorithm 2](#) to compute $\text{Log}_U^\alpha(\tilde{U})$ under the α -metric and record the wall clock computation time as well as the iteration count. The results are displayed in [Figure 13](#).

REFERENCES

- [1] P.-A. Absil, R. Mahony, and R. Sepulchre. Riemannian geometry of Grassmann manifolds with a view on algorithmic computation. *Acta Applicandae Mathematica*, 80(2):199–220, 2004.
- [2] P.-A. Absil, R. Mahony, and R. Sepulchre. *Optimization Algorithms on Matrix Manifolds*. Princeton University Press, Princeton, New Jersey, 2008.
- [3] E. Begelfor and M. Werman. Affine invariance revisited. *IEEE Conference on Computer Vision and Pattern Recognition*, 2:2087–2094, 2006.
- [4] P. Benner, S. Gugercin, and K. Willcox. A survey of projection-based model reduction methods for parametric dynamical systems. *SIAM Review*, 57(4):483–531, 2015.
- [5] A. V. Bernstein and A. P. Kuleshov. Tangent bundle manifold learning via Grassmann & Stiefel eigenmaps. *arXiv preprint arXiv:1212.6031*, 2012.
- [6] R. Bhatia. *Matrix Analysis*. Number 169 in Graduate Texts in Mathematics. Springer-Verlag, New York – Berlin – Heidelberg, 1997.
- [7] D. Bryner. Endpoint geodesics on the Stiefel manifold embedded in Euclidean space. *SIAM Journal on Matrix Analysis and Applications*, 38(4):1139–1159, 2017.
- [8] E. Celledoni, S. Eidnes, B. Owren, and T. Ringholm. *Mathematics of Computation*, (89):699–716, 2020.

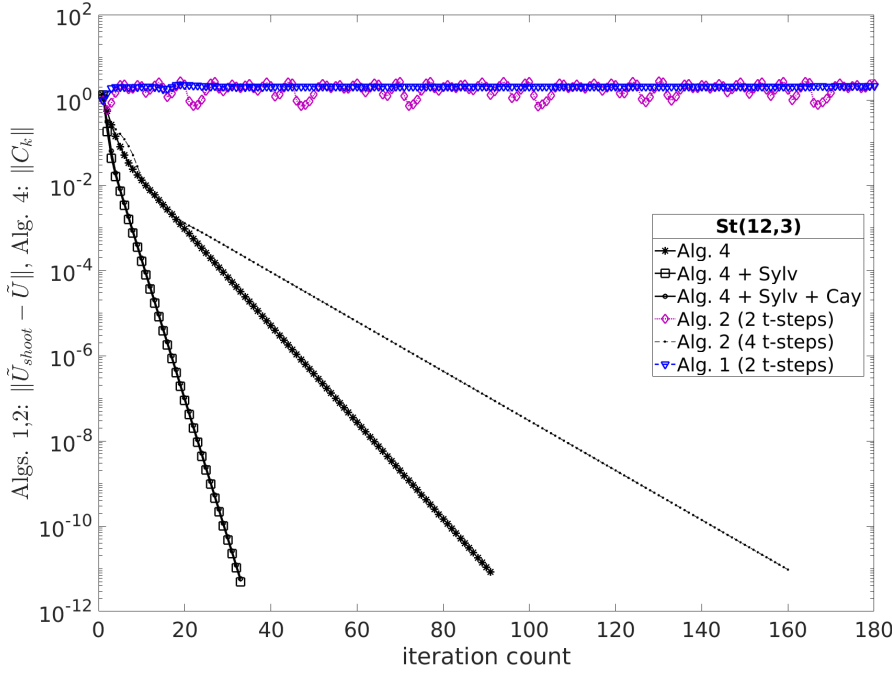


FIG. 10. (cf. Subsection 4.1) Convergence history of the various log-algorithms for computing $\text{Log}_U(\tilde{U})$ under the canonical metric. The graphs show one run of the test case $\text{St}(12, 3)$. The input data is at a Riemannian distance of $\text{dist}(U, \tilde{U}) = 0.95\pi$.

- [9] R. Chakraborty and B. C. Vemuri. Statistics on the (compact) Stiefel manifold: Theory and applications. arXiv:1708.00045v1, 2017.
- [10] M. P. do Carmo. *Riemannian Geometry*. Mathematics: Theory & Applications. Birkhäuser Boston, 1992.
- [11] A. Edelman, T. A. Arias, and S. T. Smith. The geometry of algorithms with orthogonality constraints. *SIAM Journal on Matrix Analysis and Applications*, 20(2):303–353, 1998.
- [12] K. A. Gallivan, A. Srivastava, X. Liu, and P. Van Dooren. Efficient algorithms for inferences on Grassmann manifolds. In *IEEE Workshop on Statistical Signal Processing*, pages 315–318, 2003.
- [13] R. Godement and U. Ray. *Introduction to the Theory of Lie Groups*. Universitext. Springer International Publishing, 2017.
- [14] E. Hairer, C. Lubich, and G. Wanner. *Geometric numerical integration: Structure-preserving algorithms for ordinary differential equations.*, volume 31 of *Springer Series in Computational Mathematics*. Springer-Verlag, Berlin, 2nd edition, 2006.
- [15] N. J. Higham. *Functions of Matrices: Theory and Computation*. Society for Industrial and Applied Mathematics, Philadelphia, PA, USA, 2008.
- [16] K. Hüper, M. Kleinsteuber, and F. Silva Leite. Rolling Stiefel manifolds. *International Journal of Systems Science*, 39(9):881–887, 2008.
- [17] K. Hüper, I. Markina, and F. Silva Leite. A Lagrangian approach to extremal curves on Stiefel manifolds. *Journal of Geometrical Mechanics*, 13(1):55–72, 2021.
- [18] K. Hüper and F. Ullrich. Real Stiefel manifolds: An extrinsic point of view. In *2018 13th APCA International Conference on Automatic Control and Soft Computing (CON-TROLO)*, pages 13–18, June 2018.
- [19] A. Iserles, H. Z. Munthe-Kaas, S. P. Nørsett, and A. Zanna. Lie-group methods. *Acta Numerica*, 9:215–365, 2000.
- [20] J. M. Lee. *Introduction to Riemannian Manifolds*. Graduate Texts in Mathematics. Springer International Publishing, Cham, 2nd edition, 2018.
- [21] Y. Man Lui. Advances in matrix manifolds for computer vision. *Image and Vision Computing*, 30(6–7):380–388, 2012.

- [22] H. Q. Minh and V. Murino. *Algorithmic Advances in Riemannian Geometry and Applications: For Machine Learning, Computer Vision, Statistics, and Optimization*. Advances in Computer Vision and Pattern Recognition. Springer International Publishing, Cham, 2016.
- [23] M. Müger. Notes on the theorem of Baker-Campbell-Hausdorff-Dynkin. Lecture Notes, Radboud University, April 2020. <https://www.math.ru.nl/~mueger/PDF/BCHD.pdf>.
- [24] M. Newman, S. Wasin, and R. C. Thompson. Convergence domains for the Campbell-Baker-Hausdorff formula. *Linear and Multilinear Algebra*, 24(4):301–310, 1989.
- [25] D. Nguyen. Closed-form geodesics and trust-region method to calculate Riemannian logarithms on Stiefel and its quotient manifolds. <https://arxiv.org/abs/2103.13327>, 2021.
- [26] L. Noakes. A global algorithm for geodesics. *Journal of the Australian Mathematical Society. Series A. Pure Mathematics and Statistics*, 65(1):37–50, 1998.
- [27] V. Patrangenaru and L. Ellingson. *Nonparametric Statistics on Manifolds and Their Applications to Object Data Analysis*. Chapman & Hall/CRC Monographs on Statistics & Applied Probability. CRC Press, 2015.
- [28] I. U. Rahman, I. Drori, V. C. Stodden, D. L. Donoho, and P. Schröder. Multiscale representations for manifold-valued data. *SIAM Journal on Multiscale Modeling and Simulation*, 4(4):1201–1232, 2005.
- [29] Q. Rentmeesters. *Algorithms for data fitting on some common homogeneous spaces*. PhD thesis, Université Catholique de Louvain, Louvain, Belgium, 2013.
- [30] W. Rossmann. *Lie Groups: An Introduction Through Linear Groups*. Oxford Graduate Texts in Mathematics. Oxford University Press, 2006.
- [31] Y. Saad and M. H. Schultz. GMRES: A generalized minimal residual algorithm for solving nonsymmetric linear systems. *SIAM Journal on Scientific and Statistical Computing*, 7(3):856–869, 1986.
- [32] A. Srivastava and E. P. Klassen. *Functional and Shape Data Analysis*. Springer Series in Statistics. Springer Verlag, New York, 2016.
- [33] A. Srivastava and P. K. Turaga. *Riemannian computing in computer vision*. Springer International Publishing, 2015.
- [34] Ganesh Sundaramoorthi, Andrea Mennucci, Stefano Soatto, and Anthony Yezzi. A new geometric metric in the space of curves, and applications to tracking deforming objects by prediction and filtering. *SIAM Journal on Imaging Sciences*, 4(1):109–145, 2011.
- [35] M. Sutti. *Riemannian Algorithms on the Stiefel and the Fixed-Rank Manifold*. PhD thesis, Université de Genève, 2020.
- [36] M. Sutti and B. Vandereycken. The leapfrog algorithm as nonlinear Gauss–Seidel. [arXiv:2010.14137v1](https://arxiv.org/abs/2010.14137v1), 2020.
- [37] R. C. Thompson. Convergence proof for Goldberg’s exponential series. *Linear Algebra and its Applications*, 121:3–7, 1989.
- [38] P. K. Turaga, Veeraraghavan A., and R. Chellappa. Statistical analysis on Stiefel and Grassmann manifolds with applications in computer vision. In *2008 IEEE Conference on Computer Vision and Pattern Recognition*, pages 1–8, June 2008.
- [39] A. Van-Brunt and M. Visser. Simplifying the Reinsch algorithm for the Baker-Campbell-Hausdorff series. [arXiv:1501.05034](https://arxiv.org/abs/1501.05034), 2015.
- [40] R. Z. A matrix-algebraic algorithm for the Riemannian logarithm on the Stiefel manifold under the canonical metric. *SIAM Journal on Matrix Analysis and Applications*, 38(2):322–342, 2017.
- [41] R. Z. Hermite interpolation and data processing errors on Riemannian matrix manifolds. *SIAM Journal on Scientific Computing*, 42(5):A2593–A2619, 2020.
- [42] R. Zimmermann. A note on rank-one subspace modifications and some remarks on the canonical Stiefel logarithm. In P. Grohs, O. Sander, J.-L. Starck, and J. Wallner, editors, *Nonlinear Data: Theory and Algorithms*, number 20/2018 in Oberwolfach Reports, pages 57–61, 2018.
- [43] R. Zimmermann. Manifold interpolation. In P. Benner, S. Grivet-Talocia, A. Quarteroni, G. Rozza, W. Schilders, and L. M. Silveira, editors, *System- and Data-Driven Methods and Algorithms*, volume 1 of *Model Order Reduction*, pages 229–274. De Gruyter, Boston, 2021.

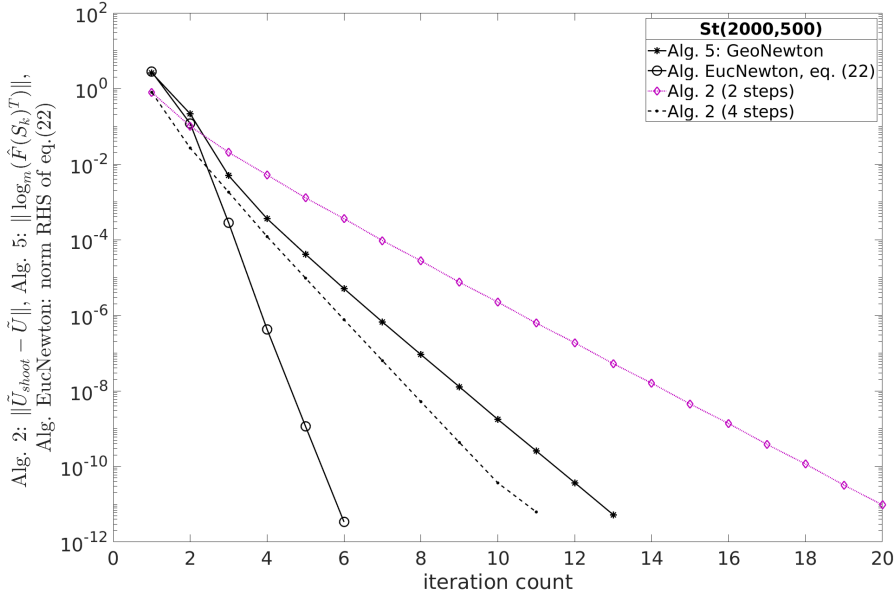


FIG. 11. (Cf. [Subsection 4.2](#)) Convergence history of the various log-algorithms for computing $\text{Log}_U(\tilde{U})$ under the Euclidean metric. The graphs show one run of the test case $St(2000, 500)$. The input data is at a Riemannian distance of $\text{dist}(U, \tilde{U}) = 5\pi$.

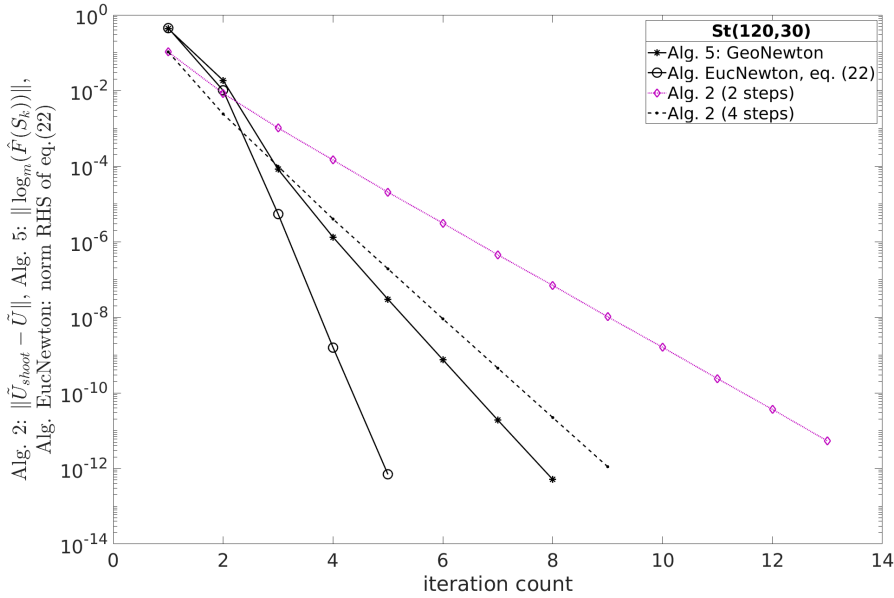


FIG. 12. (Cf. [Subsection 4.2](#)) Convergence history of the various log-algorithms for computing $\text{Log}_U(\tilde{U})$ under the Euclidean metric. The graphs show one run of the test case $St(120, 30)$. The input data is at a Riemannian distance of $\text{dist}(U, \tilde{U}) = \pi$.

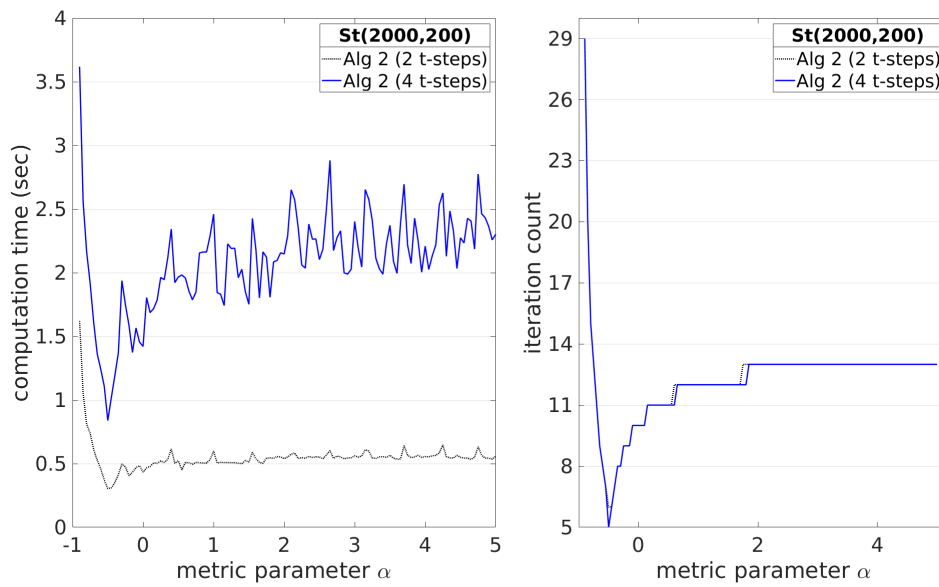


FIG. 13. (cf. [Subsection 4.3](#)) Wall clock computation time in seconds versus α (left) and iteration count until convergence versus α (right) for computing $\text{Log}_U^\alpha(\tilde{U})$ with [Algorithm 2](#). The trial parameter set is $\{\alpha = -0.9 + 0.05j \mid j = 0, \dots, 118\}$. The data points $U, \tilde{U} \in \text{St}(2000, 200)$ are at a Riemannian α -distance of $\text{dist}_\alpha(U, \tilde{U}) = 0.8\pi$. Timing results are averaged over 10 runs.